Human Molecular Genetics, 2013 **1–18**
doi:10.1093/hmg/ddt530

FOXO3 determines the accumulation of α-synuclein and controls the fate of dopaminergic neurons in the *substantia nigra*

Emilda Pino[1,†], Ryoji Amamoto[1,†], Lu Zheng[1], Matthias Cacquevel[1], Juan-Carlos Sarria[2], Graham W. Knott[3] and Bernard L. Schneider[1,*]

[1]Brain Mind Institute, Neurodegenerative Studies Laboratory, Ecole Polytechnique Fédérale de Lausanne (EPFL), Lausanne, Switzerland, [2]BioImaging and Optics Core Facility, EPFL, Lausanne, Switzerland and [3]Centre of Interdisciplinary Electron Microscopy, EPFL, Lausanne, Switzerland

Received May 16, 2013; Revised September 25, 2013; Accepted October 19, 2013

Parkinson's disease (PD) is characterized by the selective degeneration of neuronal populations presumably due to pathogenic interactions between aging and predisposing factors such as increased levels of α-synuclein. Here, we genetically modulate the activity of the transcription factor Forkhead box protein O3 (FOXO3) in adult nigral dopaminergic neurons using viral vectors and explore how this determinant of longevity impacts on neuronal fate in normal and diseased conditions. We find that dopaminergic neurons are particularly vulnerable to changes in FOXO3 activity in the *substantia nigra*. While constitutive activation has proapoptotic effects leading to neuronal loss, inhibition of FOXO-mediated transcription by a dominant-negative competitor causes oxidative damage and is detrimental at high vector dose. To address the role of FOXO3 in PD, we modulate its activity in dopaminergic neurons overexpressing human α-synuclein. In this pathogenic condition, we find that FOXO inhibition has protective effects, suggesting that this transcription factor ultimately contributes to neuronal cell death. Nevertheless, mild FOXO3 activity also protects nigral neurons against the accumulation of human α-synuclein, albeit to a lesser extent. FOXO3 reduces the amount of α-synuclein present in the soluble protein fraction and promotes the coalescence of dense proteinase K-resistant aggregates, with an accumulation of autophagic vacuoles containing lipofuscin. Consistent with these *in vivo* observations, we find that FOXO3 controls autophagic flux in neuronal cells. Altogether, these results point to FOXO3 as an important determinant of neuronal survival in the *substantia nigra*, which may oppose α-synuclein accumulation and proteotoxicity.

INTRODUCTION

Aging of the human brain is a crucial factor in the etiology of Parkinson's disease (PD), characterized by the progressive demise of vulnerable neuronal populations including nigral dopamine (DA) neurons. In particular, aging may underlie the pathogenic effect of α-synuclein, a protein prone to abnormal conformational changes (1,2) and which is associated with familial and sporadic forms of the disease (3–5).

The role of aging in neurodegenerative disorders remains elusive. Aging is often attributed to unpredictable environmental factors, leading to cumulative oxidative damage for instance (6,7). Interestingly, metabolic pathways related to calorie restriction and insulin/IGF1 signaling (IIS) determine lifespan in model organisms (8,9). The existence of intrinsic factors modifying the rate of organism senescence suggests that the same determinants may control the pathogenic processes leading to neurodegeneration.

The IIS pathway controls the activity of Forkhead box protein O transcription factors, a sub-class of the Forkhead family (10). In humans, polymorphisms in the *Forkhead box protein O3* (*FOXO3*) gene are associated with exceptional longevity (11). In the nematode *Cænorhabditis elegans*, mutations in the gene encoding the insulin/IGF1 receptor increase lifespan by

*To whom correspondence should be addressed at: Brain Mind Institute, Neurodegenerative Studies Laboratory, Ecole Polytechnique Fédérale de Lausanne (EPFL), AI 2241 Station 19, 1015 Lausanne, Switzerland. Tel: +41 216939505; Fax: +41 216939520; Email: bernard.schneider@epfl.ch
†These authors contributed equally to this study.

inactivating Akt (12,13), which results in nuclear translocation and activation of the FOXO ortholog DAF-16. Factors sensing the level of oxidative stress and energy status in the cell, such as sirtuins, further regulate FOXO transcriptional activity via posttranslational modifications including phosphorylation, acetylation and ubiquitination (10, 14–18). In mammals, depending upon environmental stimuli and tissue specificities, FOXO-driven transcription leads to contrasted effects, which span from increased resistance against oxidative stress and reduced cell cycling, to muscle atrophy and neuronal cell death (19–26). Overall, the implication of FOXO proteins in the mechanisms of aging and cellular stress resistance prompts further studies to explore their role in neurodegenerative disorders.

A recent gene expression profiling has found increased expression of FOXO1, as well as enhanced transcription of genes containing FOXO-binding sites in the prefrontal cortex of PD patients (27). Besides this direct evidence, experimental models further indicate a role for FOXO in the control of protein misfolding and aggregation, which has been implicated in various neurodegenerative disorders including PD. The accumulation and toxicity of misfolded proteins is controlled by IIS. In *C. elegans* overexpressing the amyloid β peptide (Aβ), reduced IIS delays Aβ toxicity via a subtle balance involving HSF-1 and DAF-16 transcriptomes, where DAF-16 accelerates the transition from potentially toxic oligomers to large and inert aggregates (28). Similarly, decreased IIS protects worms from polyglutamine aggregation in muscle cells, an effect mediated by DAF-16 (29).

In PD, dopaminergic neurons selectively vulnerable to neurodegeneration are chronically exposed to oxidative stress caused by DA metabolism. Depending on the type of stress to which neuronal cells are exposed, FOXO can have contrasted effects. In neural stem cells, FOXO controls the expression of detoxifying enzymes and thereby contributes to cell survival (23, 24). When neurons are exposed to acute stress, FOXO can upregulate FasL or Bim, leading to neuronal apoptosis (21, 25). Therefore, it is essential to address the role of FOXO in conditions narrowly mimicking the pathogenic context at hand.

Using a genetic approach to modulate FOXO3 activity in the adult rat *substantia nigra pars compacta* (SNpc), we determine *in vivo* how this transcription factor impacts on the survival of DA neurons. The role of FOXO3 is further investigated in a mammalian model system based on the pathogenic accumulation of α-synuclein in the nigrostriatal system, and which replicates features of early PD.

RESULTS

FOXO3 is expressed in nigral DA neurons and constitutive FOXO3 activation leads to neuronal loss

We sought to determine whether the transcription factor FOXO3 was expressed in DA neurons of the rat SNpc and how its activity affects the fate of these neurons. Immunohistochemistry for endogenous FOXO3 revealed expression in neurons positively labeled with tyrosine hydroxylase (TH) (Fig. 1A). In these neurons, FOXO3 appeared to accumulate mostly in the cell cytoplasm (arrowheads) and within few nuclei (arrows) (Fig. 1B).

To selectively modulate the activity of FOXO3 in nigral neurons, we generated serotype 6 adeno-associated viral vectors (AAV2/6) for stereotaxic injections into the SNpc. The vector AAV-FoxO3a encodes wild-type FOXO3. AAV-FoxO-TM produces a constitutively active form retained in the cell nucleus as the three Akt-dependent phosphorylation sites are mutated to alanines (30). To inhibit FOXO activity, we used the truncated AAV-FoxO-DBD vector, which encodes 139 amino acids in the FOXO3 DNA-binding region without the transactivation domain. We chose this approach to suppress FOXO transcriptional activity because FoxO-DBD is conserved among all four members of the FOXO subfamily (FOXO1, 3, 4 and 6), which have been shown to have redundant activities in rodents (31). All three constructs were HA-tagged for immunodetection.

To assess *in vitro* the functionality of these FOXO variants, we measured changes in FOXO transcriptional activity by co-transfecting the AAV constructs in HEK293T cells with a construct expressing luciferase under the control of six FOXO-binding DNA elements (Supplementary Material, Fig. S1A and B). As expected, wild-type FOXO3 significantly increased the expression of luciferase, an effect which was 7-fold increased for the nuclear FoxO-TM variant (Supplementary Material, Fig. S1A). The dominant-negative FoxO-DBD did not induce any detectable transcriptional activity. However, when co-transfected with FOXO3, it clearly suppressed the FOXO transcriptional activity in a dose-dependent manner, confirming the dominant-negative effect of FoxO-DBD (Supplementary Material, Fig. S1B).

Next, we tested the effect of modulating FOXO3 activity in conditions of acute oxidative stress, as this transcription factor has been implicated in neuronal cell death induced by reactive oxygen species (ROS) (16, 32). SH-SY5Y cells were infected with AAV vectors and later exposed to 200 μM H_2O_2 for 6 h. At 48 h after infection, apoptotic cell death was measured using Annexin V binding (Supplementary Material, Fig. S1C). In non-infected control conditions, 45.1 ± 3.3% of apoptotic cells were detected. While wild-type FOXO3 did not change this proportion (43.8 ± 1.3%), the expression of FoxO-TM significantly increased the percentage of apoptotic cells to 57.4 ± 1.5%. In contrast, the dominant-negative DBD had a protective effect against acute oxidative stress, reducing the proportion of apoptotic SH-SY5Y cells to 24.5 ± 2.2%. These results confirmed the primary proapoptotic role of FOXO in conditions of acute oxidative stress (16,32).

DA neurons in the rat SNpc are chronically exposed to low levels of oxidative stress caused by DA metabolism, and are therefore expected to respond very differently to changes in FOXO activity. To evaluate how FOXO3 activity determines the fate of DA neurons, we unilaterally injected AAV vectors into the SNpc of adult rats. As the level of transgene expression may critically influence the physiological response to FOXO, we used two different vector doses. The injection of vectors modulating FOXO3 activity was compared with control groups injected with the same dose of a vector coding for the fluorescent protein FPmax, and for each animal, the injected SNpc was compared with the non-injected side.

Three and 12 weeks post-injection of a dose of 6.7×10^6 TU, we observed expression of the transgene in a majority of nigral DA neurons, and in some neighboring non-dopaminergic

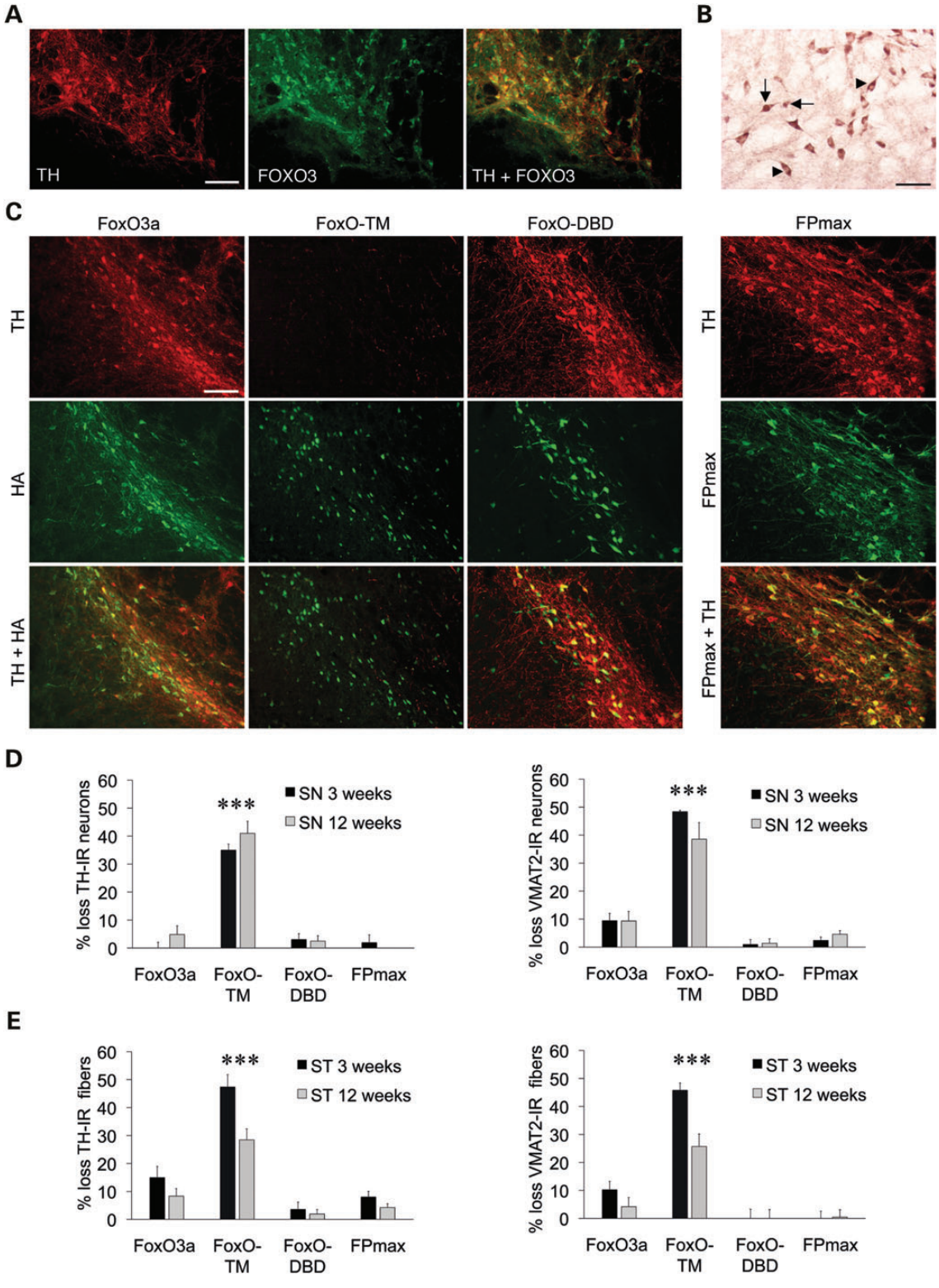

Figure 1. FOXO3 is endogenously expressed in rat nigral neurons, and constitutive FOXO3 activity leads to acute loss of neurons positive for DA markers. (**A**) Fluorescence immunostaining showing co-localization of both TH (red) and FOXO3 (green) in adult rat nigral neurons. Scale bar: 100 μm. (**B**) Immunohistochemistry for FOXO3 in the adult rat SNpc showing either predominantly nuclear (arrows) or cytoplasmic (arrowheads) localization. Scale bar: 50 μm (**C**) Immunodetection demonstrates widespread transgene expression in the adult rat SNpc (TH colabeling) 12 weeks following AAV2/6 vector injection (6.7×10^6 TU). The FOXO3 forms are immunodetected using an N-terminal fused HA epitope. Scale bar: 100 μm. (**D**) Loss of neurons positive for TH and VMAT2, as compared with the non-injected hemisphere, at 3 and 12 weeks post-vector injection. Only the constitutively active FoxO-TM leads to an acute loss of DA neurons. (**E**) Loss of TH- and VMAT2-positive fibers in the striatum. Statistical analysis: at 3 weeks, $n = 6$ in each group, except FoxO-TM ($n = 4$). At 12 weeks: FoxO3a $n = 10$, FoxO-DBD $n = 9$, FoxO-TM and FPmax $n = 8$. (D) Two-way factorial ANOVA, group effect: for TH, $F(3,49) = 62.6$ and for VMAT2, $F(3,49) = 60.0$; $^{***}P < 0.001$ relative to the other groups. (E) Two-way factorial ANOVA, group effect: for TH, $F(3,49) = 50.5$ and for VMAT2, $F(3,49) = 31.4$; $^{***}P < 0.001$ relative to the other groups.

neurons (Fig. 1C). While the number of nigral neurons positive for DA markers remained unchanged with both wild-type FOXO3 and the dominant-negative FoxO-DBD (Fig. 1D), the constitutively active form FoxO-TM induced a loss of neurons positive for either TH (35 ± 2.1%) or VMAT2 (48.4 ± 0.5%), as well as a corresponding decrease in the density of striatal DA fibers (Fig. 1E). At 12 weeks, although the extent of DA neuron loss remained similar, we measured a significant recovery of TH-positive striatal innervation (28.5 ± 3.9% loss versus 47.4 ± 4.4% at Week 3). A similar recovery was observed for the DA marker VMAT2 (Fig. 1D and E).

These results indicate that mild levels of FOXO3 activation or inhibition do not significantly affect the survival of DA neurons in the SNpc. However, constitutive FOXO3 activation precipitates the loss of neurons and their striatal projections.

High dose of the dominant-negative FoxO-DBD leads to oxidative damage and loss of neurons expressing DA markers

In order to further modulate FOXO3 activity, we injected a four-time higher dose (2.7×10^7 TU) of vector and similarly measured nigral neuron survival. In animals injected with the control vector AAV-FPmax, >90% of the TH-positive neurons and fibers remained intact when compared with the non-injected side (Fig. 2A and B). With this high vector dose, wild-type FOXO3, the constitutively active form as well as the dominant-negative FoxO-DBD induced a significant loss of neurons and striatal nerve terminals positive for TH (SNpc: FoxO3a 31 ± 3.4%, FoxO-TM 43.1 ± 3.8%, FoxO-DBD 28.6 ± 2.4%) as early as 3 weeks post-injection. The loss of SNpc neurons positive for VMAT2 confirmed these results (FoxO3a 34.9 ± 4.4%, FoxO-TM 58.3 ± 4.4%, FoxO-DBD 42.7 ± 5.1%). In all the conditions leading to the loss of neurons positive for DA markers, cleaved Caspase 9 was detected in TH-positive neurons (Fig. 2C). The activation of this apoptotic marker and the similar loss of the DA markers TH and VMAT2 suggest that nigral neurons undergo terminal degeneration. Overall, nigral neurons appear highly vulnerable to major changes in FOXO3 activity.

Next, we explored the cause of neuronal loss induced by the dominant-negative FOXO-DBD. The physiological role of FOXO transcription factors has been linked to resistance against oxidative stress in quiescent cells (22, 31). Hence, we assessed the presence of oxidative damage in the injected ventral midbrain. Remarkably, only the SNpc injected with the FoxO-DBD vector showed positive immunostaining for 4-hydroxynonenal (HNE), a product of lipid peroxidation (Fig. 2D). Although the possible gain of toxic functions by FOXO-DBD cannot be ruled out, ROS-induced damage in the FOXO-DBD condition is likely the consequence of inhibiting FOXO transcriptional activity and highlights the role of FOXO in neuronal resistance against oxidative stress. While FOXO3 activity can precipitate cell loss following acute oxidative damage (Supplementary Material, Fig. S1C), these results suggest that FOXO transcriptional activity rather contributes to ROS detoxification in nigral neurons chronically exposed to mild oxidative stress.

Pallidal parvalbumin neurons are not vulnerable to changes in the level of FOXO3 activity

Next, we asked whether DA neurons are selectively vulnerable to alterations in FOXO3 activity. Similar vector injections were performed in the *globus pallidus* (GP). To replicate the conditions that are detrimental to nigral neurons, we injected the low viral dose (6.7×10^6 TU) for vectors expressing FOXO3 and FoxO-TM and the high dose (2.7×10^7 TU) for the dominant-negative FoxO-DBD. The injected GP was compared with the non-injected side and to control groups injected with the same dose of the FPmax vector. Expression of the HA-tagged transgene product (FOXO3) could be detected within pallidal GABAergic neurons positive for the marker parvalbumin (PV) (Fig. 3A). Remarkably, the number of PV-positive neurons in the GP remained unchanged as compared with the non-injected side, for each of the vectors tested (Fig. 3B–D). For statistical comparison, the loss of neurons positive for the marker VMAT2 observed following nigral injections is indicated in Figure 3C and D. As compared with PV-positive neurons in the GP, nigral neurons are clearly more vulnerable to changes in FOXO3 activity. Therefore, we explored how FOXO3 determines the fate of neurons exposed to chronic stress in the context of PD.

FOXO3 and FoxO-DBD protect against the loss of nigral DA neurons induced by overexpression of human α-synuclein

As genetic anomalies leading to high levels of α-synuclein expression segregate with familial forms of PD, we induced pathogenic conditions by overexpressing human α-synuclein in the rat SNpc. AAV2/6 vectors modulating FOXO3 activity (each at a dose of 6.7×10^6 TU) were co-injected together with an AAV2/6 vector encoding α-synuclein (1.4×10^7 TU). Immunohistochemistry 3 months post-injection confirmed the robust expression of both transgenes throughout the SNpc (Fig. 4A). To assess the effect of FOXO3 on α-synuclein-induced nigral degeneration, we quantified the loss of TH-positive DA neurons in the injected SNpc versus the non-injected hemisphere (Fig. 4B and C). α-Synuclein expression induced a 26.6 ± 5% loss of neurons positive for TH when co-injected with the control vector AAV-FPmax. Predictably, the co-expression of FoxO-TM enhanced neuron loss, reaching 52.4 ± 4.1%. Remarkably, expression of both wild-type FOXO3 and the dominant-negative DBD had a protective effect on TH-positive neurons. FOXO3 preserved about half of the neurons, resulting in a 13.6 ± 3.9% loss. On the other hand, the AAV-FoxO-DBD vector conferred almost complete protection, with only 2.6 ± 1.5% loss of TH-positive neurons.

Densitometric analysis of striatal TH immunoreactivity revealed a 27.2 ± 5.9% loss in rats expressing FoxO-TM and human α-synuclein (Fig. 4D). The degree of TH loss was significantly increased with AAV-FoxO-TM with regard to any of the other vectors. Although we measured a trend towards protection by the dominant-negative FoxO-DBD, the loss of striatal TH immunoreactivity in the groups FoxO3a/α-synuclein (10.7 ± 2.8%) and FPmax/α-synuclein (10.2 ± 2.5%) was too low to demonstrate any significant difference.

We explored whether loss of the DA marker TH would coincide with signs of neuronal apoptosis 3 months post-injection of

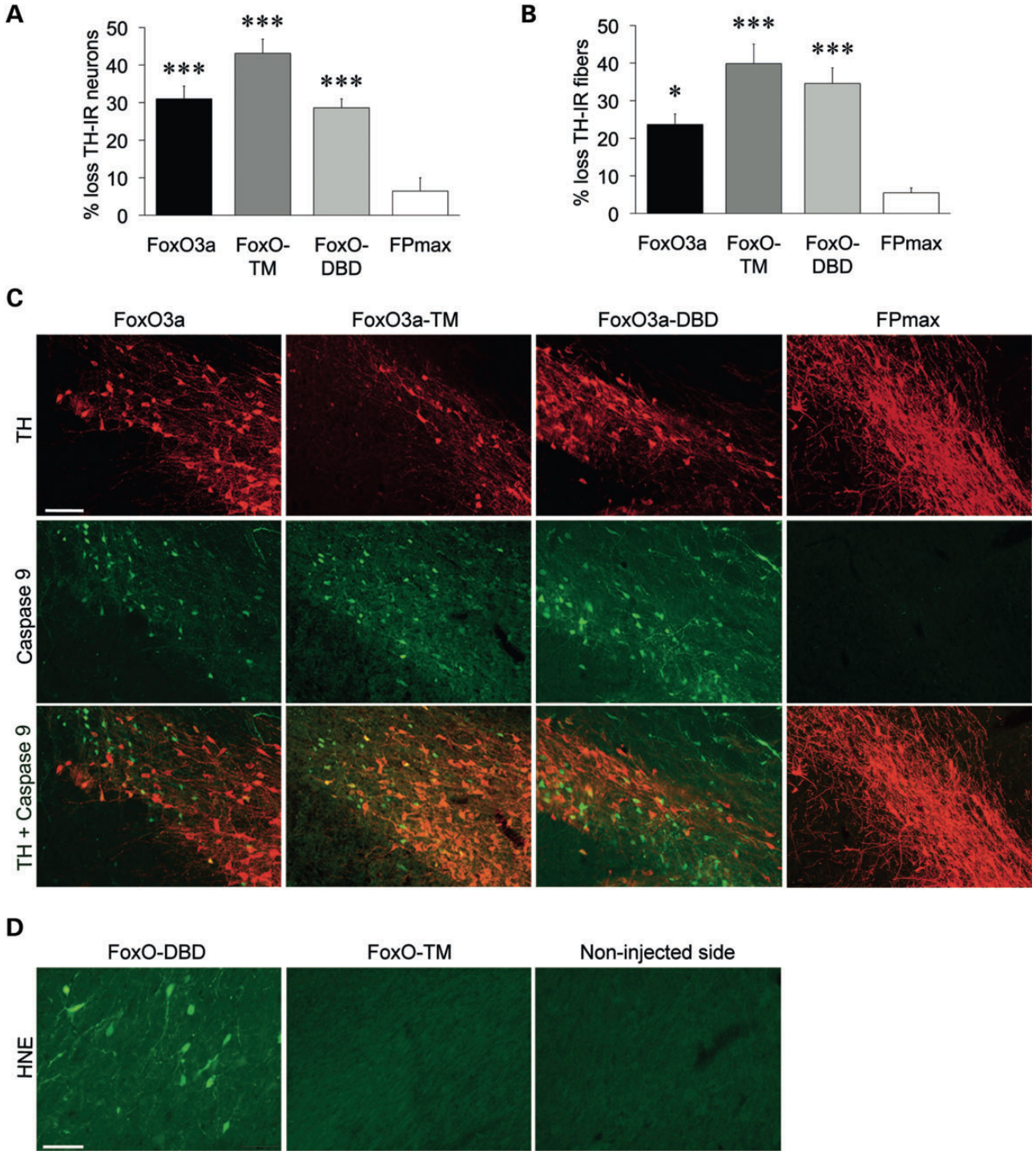

Figure 2. At a higher vector dose, all forms of FOXO3 lead to the loss of nigral neurons positive for DA markers and the dominant-negative FoxO-DBD produces oxidative damage. Significant loss of TH-positive neurons (**A**) and fibers (**B**) 3 weeks following injection of a high dose (2.7×10^7 TU) of AAV2/6 vectors modulating FOXO3 activity. Results represent the percentage loss of TH-positive neurons or TH striatal immunoreactivity, as compared with the contralateral non-injected hemisphere. Note that the FoxO3a and FoxO-DBD vectors also induce the loss of DA neurons with a high vector dose. Statistical analysis: FoxO3a $n = 10$, FoxO-TM $n = 15$, FoxO-DBD $n = 9$ and FPmax $n = 6$. (A) One-way ANOVA $F(3,36) = 14.7$: $^{***}P < 0.001$ relative to the FPmax control. (B) One-way ANOVA $F(3,36) = 8.9$: $^{*}P = 0.012$, $^{***}P < 0.001$ relative to the FPmax control. (**C**) Activation of the apoptotic marker Caspase 9 in nigral TH-positive neurons. Note the presence of cleaved Caspase 9 with the vectors modulating FOXO3 activity. Scale bar: 100 μm (**D**) Immunostaining for HNE in the SNpc of FoxO-DBD-injected rats. Note that FoxO-TM does not induce any HNE accumulation despite a similar level of toxicity. Scale bar: 50 μm.

the α-synuclein vector. Although cleaved Caspase-9 could not be detected at this latter stage (data not shown), a positive staining for activated Bax was observed in groups presenting a mild degeneration, injected either with the wild-type form of FOXO3 or the control FPmax (Supplementary Material, Fig. S2). Further indicating the occurrence of neuronal

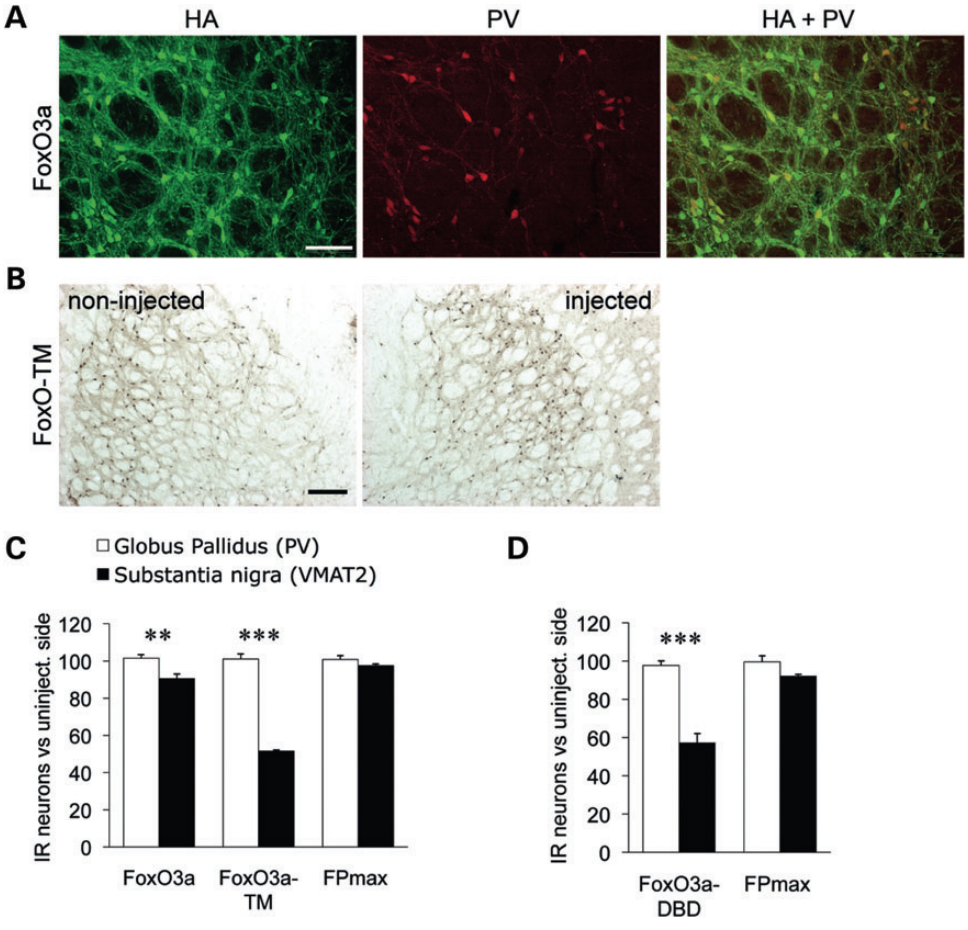

Figure 3. Pallidal PV neurons are less vulnerable to modulation of FOXO3 activity. AAV2/6 vectors modulating FOXO3 activity and the control FPmax vector were injected in the GP, analyzed 3 weeks later. (**A**) Immunostaining for HA in the GP demonstrating overexpression of FOXO3 in parvalbumin-positive (PV-IR) neurons. Scale bar: 100 μm. (**B**) PV immunohistochemistry in the GP of a FoxO-TM-injected rat. Note the similar number of PV-IR neurons in both the injected and non-injected sides. Scale bar: 200 μm. (**C**) Quantitative analysis of PV-IR and TH-IR neurons in the GP and SNpc, respectively. AAV2/6 vectors encoding FoxO3a, FoxO-TM or FPmax were injected either in GP or in SNpc (6.7×10^6 TU). Results are expressed as the percentage of immunoreactive neurons versus the non-injected hemisphere. (**D**) Similar results obtained following injection of FoxO-DBD and the control FPmax vector at a higher dose (2.7×10^7 TU). Note that PV-IR pallidal neurons were significantly less affected when compared with nigral neurons. Statistical analysis: SN: $n = 6$ for each group except FoxO-TM ($n = 4$) and FoxO-DBD ($n = 9$). GP: $n = 6$ for each group. (C) Two-way factorial ANOVA, significant interaction gene × brain region: $F(2,28) = 64.2$; $^{**}P = 0.008$ and $^{***}P = 0.0001$, comparing neuronal loss between SN and GP. (D) Two-way factorial ANOVA, significant interaction gene × brain region: $F(1,23) = 16.9$; $^{***}P = 0.0001$, comparing neuronal loss between SN and GP.

degeneration in these conditions, co-staining for activated Bax and the DA marker TH provided evidence for an on-going apoptotic response in nigral neurons.

Altogether, these data demonstrate that FOXO3 activation determines neuronal fate in response to the accumulation of α-synuclein. Interestingly, both the overexpression of wild-type FOXO3 and FoxO-DBD demonstrate significant protection of nigral cell bodies.

FOXO3 mediates the formation of dense α-synuclein aggregates in the nigrostriatal system

Next, we explored how FOXO3 modifies α-synuclein toxicity in nigral DA neurons. As subcellular distribution is an important parameter regulating FOXO3 activity, we determined whether any significant change occurred in the localization of FOXO3 and α-synuclein in the cytosolic versus nuclear compartments of nigral neurons. Quantitative confocal immunofluorescence analysis revealed neither any effect of FOXO3 on α-synuclein distribution, nor any significant change in FOXO3 localization when α-synuclein was co-expressed (Supplementary Material, Fig. S3).

Next, we investigated the effect of FOXO3 on the formation of α-synuclein aggregates in the SNpc of the injected animals. We analyzed α-synuclein accumulation in nigral cell bodies using Thioflavin S (ThioS), a dye which undergoes a characteristic shift in its excitation spectrum in the presence of β-pleated amyloid sheets (Supplementary Material, Fig. S4). A punctate ThioS signal partially colocalizing with immunostained human α-synuclein was observed in neuronal cell soma and within neurites (Supplementary Material, Fig. S4A). Twelve weeks after vector injection, we quantified the number of ThioS-positive signals per millimetre square of tissue section in the SNpc. We observed an approximate doubling in the amount of ThioS-positive aggregates per millimetre square in the FoxO-TM

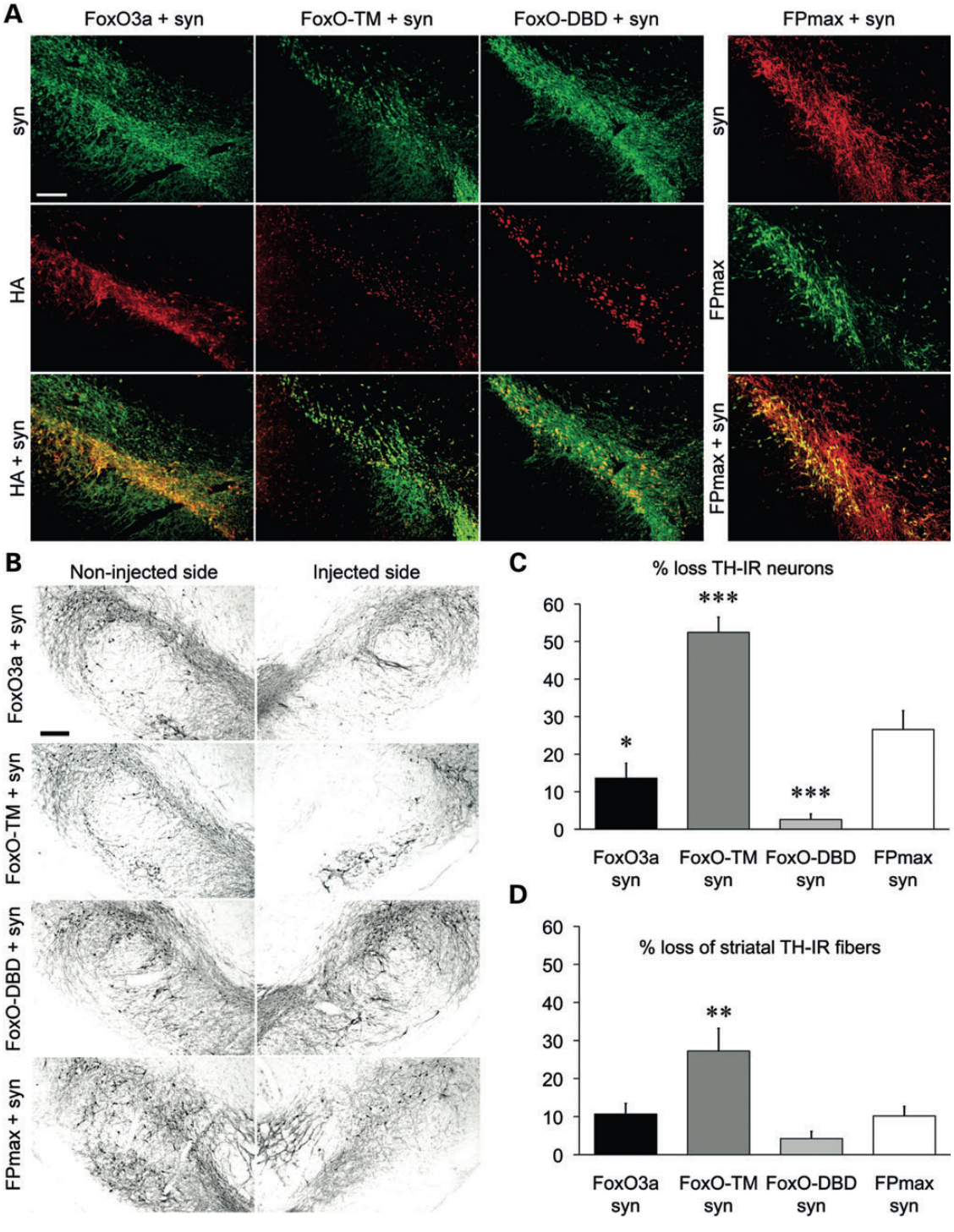

Figure 4. FOXO3 activity determines the fate of nigral DA neurons overexpressing human α-synuclein. (**A**) Immunostaining for α-synuclein and FOXO3 variants (HA) 12 weeks post-vector injection demonstrates co-expression of both transgenes in the adult rat SNpc. Scale bar: 200 μm. (**B**) Representative photomicrographs showing TH-IR neurons in the SNpc. Scale bar: 200 μm. (**C**) Loss of TH-IR neurons expressed as the percentage of the non-injected hemisphere. The AAV2/6-α-synuclein vector was co-injected with vectors modulating FOXO3 activity. FoxO-TM overexpression leads to increased loss of DA neurons, while a significant protection is observed with FoxO3a and FoxO-DBD. (**D**) Loss of DA fibers in the striatum measured by TH immunoreactivity. Statistical analysis: FoxO3a and FoxO-TM: $n = 10$, FoxO-DBD and FPmax: $n = 9$. (C) One-way ANOVA: $F(3,34) = 31.3$; $^{*}P = 0.024$, $^{***}P < 0.001$ relative to FPmax. (D) One-way ANOVA: $F(3,34) = 7.0$; $^{**}P = 0.008$ relative to FPmax.

condition, significantly different from the control group FPmax/α-synuclein (Supplementary Material, Fig. S4B and C). In the other groups, the abundance of ThioS-positive signals remained similar to the FPmax control. ThioS-positive signals displayed a larger size when FOXO3 activity was increased, prompting further histological analysis of α-synuclein aggregates.

Using another cohort of rats similarly injected with AAV2/6 vectors, we sought for the presence of aggregated forms of α-synuclein, which were immunostained on brain tissue sections previously subjected to proteinase K (PK) treatment (Fig. 5A). In the absence of PK treatment, immunostaining for human α-synuclein appeared very similar in all conditions (Fig. 5A). Remarkably, PK revealed a striking difference in the distribution of treatment-resistant forms of α-synuclein. Active forms of FOXO3 (FoxO3a and FoxO-TM) induced the formation of densely stained, PK-resistant inclusions localized in distinct portions of the cytosol (Fig. 5A). PK-resistant α-synuclein appeared highly condensed in the neuronal soma, while it was nearly absent from striatal fibers, where only a fine and punctate distribution of the staining was observed (Fig. 5A). In contrast, an abundant and diffuse distribution of PK-resistant α-synuclein was found in the FoxO-DBD/α-synuclein and control FPmax/α-synuclein groups. Alpha-synuclein staining was filling the entire cytosol, and a widespread accumulation of PK-resistant α-synuclein was similarly observed in dystrophic neurites within the striatal neuropil (Fig. 5A).

Overall, vectors enhancing FOXO3 activity lead to condensation of aggregated forms of α-synuclein in the neuronal soma, which may indicate changes in the accumulation of human α-synuclein. Therefore, we biochemically characterized α-synuclein levels in the rat midbrain.

FOXO3 activation coincides with a reduction of α-synuclein accumulation in the soluble protein fractions

To biochemically determine how FOXO3 affects α-synuclein accumulation, we performed semi-quantitative western blot analysis following three-step sequential extractions of proteins from midbrain tissue.

Comparing the total level of α-synuclein in the injected SN with the level of endogenous α-synuclein in the non-injected side, we found an approximate doubling of α-synuclein expression following AAV-α-synuclein vector injection (Supplementary Material, Fig. S5A). Human α-synuclein was mainly present in the Hepes and NP40 fractions, with little additional α-synuclein found in the SDS fraction. Immunodetection for TH, APP and histone showed the relative presence of proteins of cytosolic, membrane and nuclear origin, in each of the fractions analyzed (Supplementary Material, Fig. S5B).

Immunodetection for total α-synuclein (rat and human) revealed a reduction in the monomeric form both in the Hepes (fraction I) and NP40-soluble (fraction II) extracts when α-synuclein was coexpressed with the active forms of FOXO3 (FoxO3a and FoxO-TM; Fig. 5B). Normalization against the α-tubulin protein and the DA marker TH both substantiated an ∼50% reduction in total monomeric α-synuclein in the FoxO3a and FoxO-TM extracts when compared with the FPmax control. With FoxO-DBD, the level of α-synuclein in these two fractions appeared similar to control animals (Fig. 5C and D). Few α-synuclein could be detected in the SDS-soluble fraction in any of the conditions tested.

To assess the presence of higher molecular weight (HMW) species resulting from α-synuclein oligomerization and aggregation, western blots were carried out on the SDS-insoluble fraction solubilized in guanidine. Overexpressed α-synuclein appeared as a monomer of ∼14 kDa and HMW broad smear in all injected animals. The total amount of aggregated α-synuclein did not appear to consistently vary between all conditions tested (Fig. 5E).

Finally, we separated the Hepes-soluble protein fraction in native conditions to further analyze the α-synuclein species present in this fraction (Fig. 5F). For immunodetection, we used the syn211 antibody specifically recognizing the human protein. Alpha-synuclein migrated at an apparent approximate molecular weight of 66 kDa. On a SDS–PAGE gel, this 66 kDa band migrated at the expected α-synuclein size of 14 kDa (Fig. 5G). Therefore, human α-synuclein expressed in the soluble brain protein fraction migrates as a single species in native conditions and the amount of this apparent 66 kDa species is clearly decreased in conditions of enhanced FOXO3 activity (Fig. 5G). In contrast, FoxO-DBD seemingly increased the abundance of this α-synuclein species.

In conclusion, human α-synuclein expression leads to the accumulation of both a monomeric form and HMW species within nigral neurons. Remarkably, FOXO3 induces a clear reduction in the amount of Hepes- and NP40-soluble monomeric forms of α-synuclein, either cytosolic or loosely associated with biological membranes. Although FOXO3 does not ultimately modify the level of aggregated α-synuclein, it contributes upstream to the clearance of the more soluble α-synuclein fraction.

FoxO-TM enhances the formation of autophagic vacuoles similar to lipofuscin granules

The presence of PK-resistant dense α-synuclein aggregates prompted further examination of nigral DA neurons at the ultrastructural level. Electron microscopy with immunogold labeling (immuno-electron microscopy, IEM) for human α-synuclein revealed the presence of neuronal cell bodies densely stained with gold particles in the injected SNpc.

In these neurons, amorphous condensed material was found in distinct portions of the cytosol (Fig. 6A). At higher magnification, these structures displayed a delimiting membrane characteristic of autophagic vacuoles (Fig. 6B). Although α-synuclein immunostaining was generally observed in close proximity to this material, it was not possible to detect α-synuclein inside such dense structures because of the pre-embedding staining procedure. Many of these vacuoles appeared associated with electron lucent organelles similar to lipid droplets. The ultrastructure of these autophagic vacuoles closely resembles granules filled with lipofuscin or neuromelanin, which consist of proteins and lipids mainly derived from degenerating mitochondria or oxidized catecholamine products (33).

In line with the presence of dense ThioS-positive and PK-resistant aggregates, we observed a massive accumulation of autophagic vacuoles in the cytosol of FoxO-TM/α-synuclein neurons (Fig. 6A). Quantitative analysis revealed an ∼5-fold increase in the density of these structures when compared with the control group FPmax/α-synuclein (Fig. 6C). Although similar structures could also be observed within DA neurons in any of the conditions tested, including the non-injected SNpc, we found dense clusters of vacuoles only in the FoxO-TM animal. In contrast, small-sized autophagic granules were scattered in the neuronal cytosol in the animal injected with FoxO-DBD. A co-staining for the autophagic marker LC3 and the DA marker TH further indicated the neuronal accumulation of LC3-positive

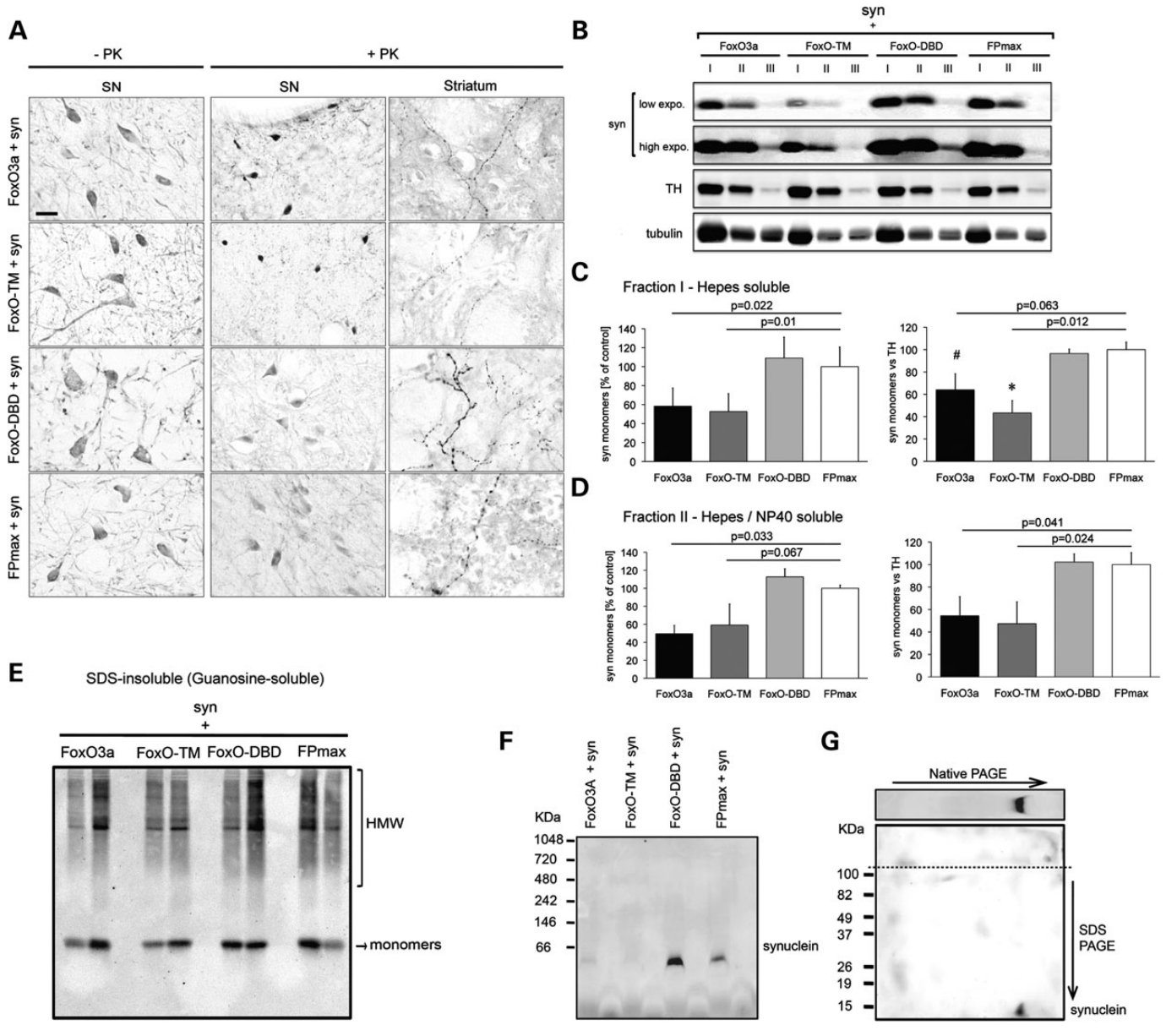

Figure 5. FOXO3 activity determines the accumulation and aggregation of α-synuclein in the nigrostriatal system. (**A**) Active forms of FOXO3 (FoxO3a and FoxO-TM) lead to the formation of dense PK-resistant structures positive for α-synuclein in the neuronal soma. In contrast, nigral neurons expressing FoxO-DBD display a diffuse accumulation of PK-resistant α-synuclein. Striatal axons show a similar difference in the pattern of PK-resistant α-synuclein. Scale bar: 20 μm. (**B**) Western blot analysis of α-synuclein accumulation in the SN of injected animals. The membrane was probed with anti-α-synuclein (syn1), anti-TH and anti-α-tubulin antibodies. Note that FoxO3a and FoxO-TM decrease the level of monomeric α-synuclein in fraction I (Hepes) and II (NP40 1%). Fraction III contains SDS-soluble proteins. (**C**, **D**) Semi-quantitative evaluation of monomeric α-synuclein detected in the Hepes (C) and NP40 fractions (D). Results are expressed as a ratio of either α-synuclein/tubulin (left panel) or α-synuclein/TH optical density (right panel). Statistical analysis: $n = 3$ for each condition, one-way ANOVA with Fisher's LSD *post hoc* test: *P*-values relative to the FPmax control are indicated on each graph. (**E**) Immunodetection of α-synuclein in the insoluble fraction (guanidine) using the syn1 monoclonal antibody. A western blot representative of two animals per group is shown. The arrow identifies monomeric α-synuclein and the bracket HMW species. (**F**) Blue native PAGE gel separation of SNpc protein extracts solubilized in Hepes. Syn211 antibody recognizes human α-synuclein migrating at an apparent molecular size of 66 kDa. Note the reduced level of α-synuclein detected in the FoxO3a and FoxO-TM conditions. Conversely, FoxO-DBD increases α-synuclein accumulation. (**G**) 2D gel separation (native and SDS-PAGE) of Hepes-soluble proteins from a FoxO-DBD extract. Immunodetection identifies α-synuclein migrating at an apparent molecular weight of 66 kDa in native conditions and 14 kDa in denaturing conditions (syn1 antibody).

punctate structures in the FoxO3a and FoxO-TM animals (Supplementary Material, Fig. S6). Altogether, these results confirmed that FOXO3 activity promotes the condensation of insoluble material in neuronal cytosol.

Interestingly, we observed a 50% reduction in the cytosolic density of mitochondria in the FoxO-TM condition, as compared with the control FPmax/α-synuclein (Fig. 6D and E). In the other conditions, the number of mitochondria inside neurons remained similar to control, despite the presence of figures indicative of degenerating mitochondria (Fig. 6F). FOXO3-induced changes in the number of autophagic granules and mitochondria prompted further investigation on autophagic activity.

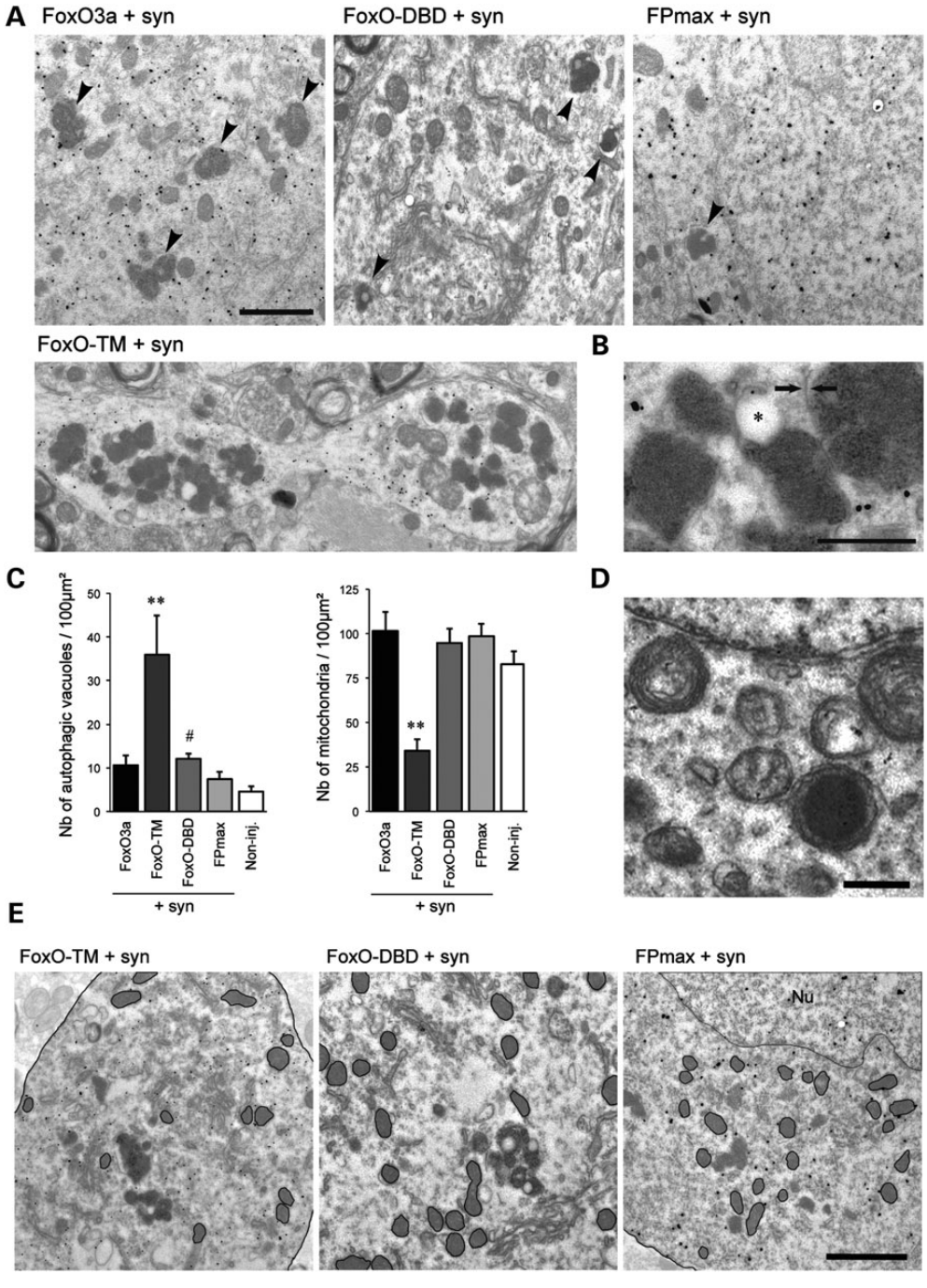

Figure 6. IEM reveals signs of enhanced autophagy in response to the constitutively active FoxO-TM. (**A**) Representative IEM of nigral DA neurons expressing human α-synuclein, showing the presence of autophagic structures with an electron dense matrix (arrowheads) in the cytosol. Note the presence of immunogold particles labeling human α-synuclein. In the FoxO-TM animal, there is a dense accumulation of autophagic vacuoles in discrete portions of the cytosol. Scale bar: 2 μm (**B**) Higher magnification of autophagic vacuoles. Note the presence of a single membrane (arrows) and a lipid droplet (*) typical of lipofuscin granules. Scale bar: 1 μm. (**C**) Quantitative IEM analysis of autophagic vacuole density in neuronal cytosol 16 weeks post-vector injection. The number of autophagic vacuoles per 100 μm^2 is significantly increased in the FoxO-TM condition. In response to FoxO-DBD, there is a trend toward increased density. Statistical analysis: $n = 17/20/46/18/20$ for FoxO3a/FoxO-TM/FoxO-DBD/FPmax/non-injected, Kruskal–Wallis one-way ANOVA: $\#P = 0.073$, $^{**}P = 0.0035$ relative to FPmax (both groups, $P < 0.001$ versus non-injected). (**D**) Mitochondria density is significantly decreased in nigral neurons expressing FoxO-TM. Statistical analysis: $n = 13/21/28/22/17$ for FoxO3a/FoxO-TM/FoxO-DBD/FPmax/non-injected, Kruskal–Wallis one-way ANOVA: $^{**}P < 0.01$ relative to all groups. (**E**) Representative IEM images showing a decreased number of mitochondria with FoxO-TM. Nu indicates the nucleus. Scale bar: 2 μm (**F**) Higher magnification of a FoxO-DBD/α-synuclein neuron showing degenerating mitochondria with discontinuous outer and inner membranes. Note the mitochondrial condensation in dense osmophilic pigments. Scale bar: 1 μm.

FOXO3 activity induces an increase in autophagic flux *in vitro*, while FoxO-DBD inhibits autophagosome elimination

To examine the role of FOXO3 in autophagy induction, we moved to an *in vitro* system utilizing human neuroblastoma SH-SY5Y cells. First, the cells were infected with a control AAV-DsRed vector, AAV-α-synuclein or the AAV-FoxO3a vector, which was also used in combination with AAV-α-synuclein. To monitor the level of autophagy, we measured by western blotting the ratio between the autophagosome-associated LC3-II, which is conjugated to phosphatidylethanolamine (PE), and the LC3-I precursor. We found that overexpression of α-synuclein led to an increase in the LC3-II/LC3-I ratio (Supplementary Material, Fig. S7A), as reported previously (34). As the level of LC3-II was increased in the cells overexpressing α-synuclein (+60%), it is however possible that lysosomal degradation is impaired in this condition. FoxO3a similarly increased the LC3-II/LC3-I ratio, although without any accumulation of LC3-II, which is consistent with increased autophagic flux (Supplementary Material, Fig. S7A). The LC3-II/LC3-I ratio was also increased when FoxO3a and α-synuclein were coexpressed.

Next, we compared the effect of the various FOXO variants (Supplementary Material, Fig. S7B). As compared with the AAV-FoxO3a vector, the constitutively active FoxO-TM further increased the LC3-II/LC3-I ratio, suggesting even higher autophagic activity. For the dominant-negative FoxO-DBD, the LC3-II/LC3-I ratio was comparable to FoxO3a, although with a higher level of LC3-II possibly indicating a reduction in autophagic flux. When measuring the level of p62 (sequestosome 1, SQSTM1) as a marker of autophagic flux, we however did not find any significant difference between conditions ($P = 0.22$; Supplementary Material, Fig. S7B). Nevertheless, as compared with FoxO3a, the p62 signal tend to be higher for FoxO-DBD and lower for FoxO-TM, again suggesting mild variations in autophagic flux that are consistent with FOXO3 activity.

Based on these initial indications for a role of FOXO3 in autophagy, we further investigated the effect of FOXO3 following α-synuclein overexpression in neuroblastoma cells, in order to replicate the conditions tested *in vivo*. As changes in the level of LC3-I and LC3-II suggest that α-synuclein could affect autophagic activity, we used several methods to determine if FOXO3 was able to increase autophagic flux in cells exposed to α-synuclein accumulation. First, the number of autophagosomes was determined using EGFP-tagged LC3, which binds to the inner and outer membranes of autophagosomes following C-terminal cleavage by Atg4 and conjugation to PE. The number of EGFP-LC3 puncta is regarded as a reliable measure of the number of autophagosomes (35). In all conditions, the cells were cotransduced with AAV-α-synuclein. Compared with the DsRed control, FoxO3a and FoxO-TM increased the number of EGFP-LC3 puncta per cell near the level of the positive control, a nutrient deprivation condition treated with Bafilomycin A1 (BA), an inhibitor of lysosomal degradation (Fig. 7A). Interestingly, FoxO-DBD also led to a significant increase in autophagosome density, similar to our *in vivo* observation. To control for indiscriminate EGFP puncta, we used EGFP-LC3 G120A, which is defective in conjugating to PE and thus, autophagosomes (36). With this construct, none of the conditions exerted a significant effect over the control.

Next, we specifically assessed changes in autophagic flux. First, the number of autophagosomes was indirectly assessed by immunoblotting the infected SH-SY5Y protein extracts with an anti-LC3B antibody for detection of LC3-I and LC3-II. We monitored autophagic flux by measuring the difference in band intensity with and without BA. With this assay, we found that all forms of FOXO3 increased the ratio of LC3-II/tubulin band intensity when subjected to BA treatment compared with the DsRed control, which suggests that the number of autophagosomes is indeed increased in all conditions (Fig. 7B). However, although we found a difference with and without BA in both FoxO3a and FoxO-TM, there was no such difference with the dominant-negative FoxO-DBD, indicating that FoxO-DBD increases the number of autophagosomes by inhibiting lysosomal degradation.

Next, we generated stable SH-SY5Y cell lines expressing either EGFP-LC3 or EGFP-LC3 G120A. During the process of autophagy, EGFP-LC3 is selectively degraded or the EGFP signal is quenched as it reaches the lysosome (37). Flow cytometry for EGFP showed that the proportion of highly fluorescent cells was reduced in response to FoxO3a and FoxO-TM (Fig. 7C). With FoxO-DBD, EGFP fluorescence remained similar to the DsRed control (open traces), suggesting that the cells infected with FoxO-DBD do not efficiently degrade EGFP-LC3 in their lysosomes. In the EGFP-LC3 G120A cells, the fluorescence level remained equivalent to control except for FoxO-TM, as apoptosis induced in this condition likely reduced EGFP fluorescence.

This result was confirmed by immunoblotting protein extracts of the same EGFP-LC3 cells with an anti-GFP antibody. Since LC3 is more susceptible to degradation than EGFP, free EGFP protein appears as a product of lysosomal EGFP-LC3 degradation (38). Therefore, the level of free EGFP is an indicator of autophagic flux. Clearly, we observed a reduction in free EGFP accumulation with FoxO-DBD compared with DsRed, contrasting with the FoxO3a and FoxO-TM conditions (Fig. 7D).

Taken together, these results show that autophagic flux is increased with FoxO3a and FoxO-TM, also in conditions where α-synuclein is overexpressed. In contrast, FoxO-DBD increases the number of autophagosomes by inhibiting lysosomal degradation.

Foxo3a and FoxO-TM lead to a reduction of mitochondria content in SH-SY5Y cells expressing α-synuclein

We previously saw a reduction in the number of mitochondria with FoxO-TM as quantified by IEM *in vivo* (Fig. 6A). To assess the mitochondrial content *in vitro*, we generated a stable SH-SY5Y cell line expressing the mitochondrial marker Mito-DsRed2 and injected the cells with the vectors modulating FOXO activity. At 48 h post-infection, FoxO-TM displayed a cytosolic distribution, and the mitochondria content remained similar in all conditions (Supplementary Material, Fig. S8A). At 72 h, however, the distribution of FoxO-TM became mainly nuclear, and a dramatic decrease in mitochondria content was detected, to the extent that no puncta were visible (Fig. 8A). Additionally, the fluorescence of Mito-DsRed appeared lowered in a fraction of the cells with FoxO3a.

Using flow cytometry, we indirectly quantified the number of mitochondria by assessing the fluorescence signal of

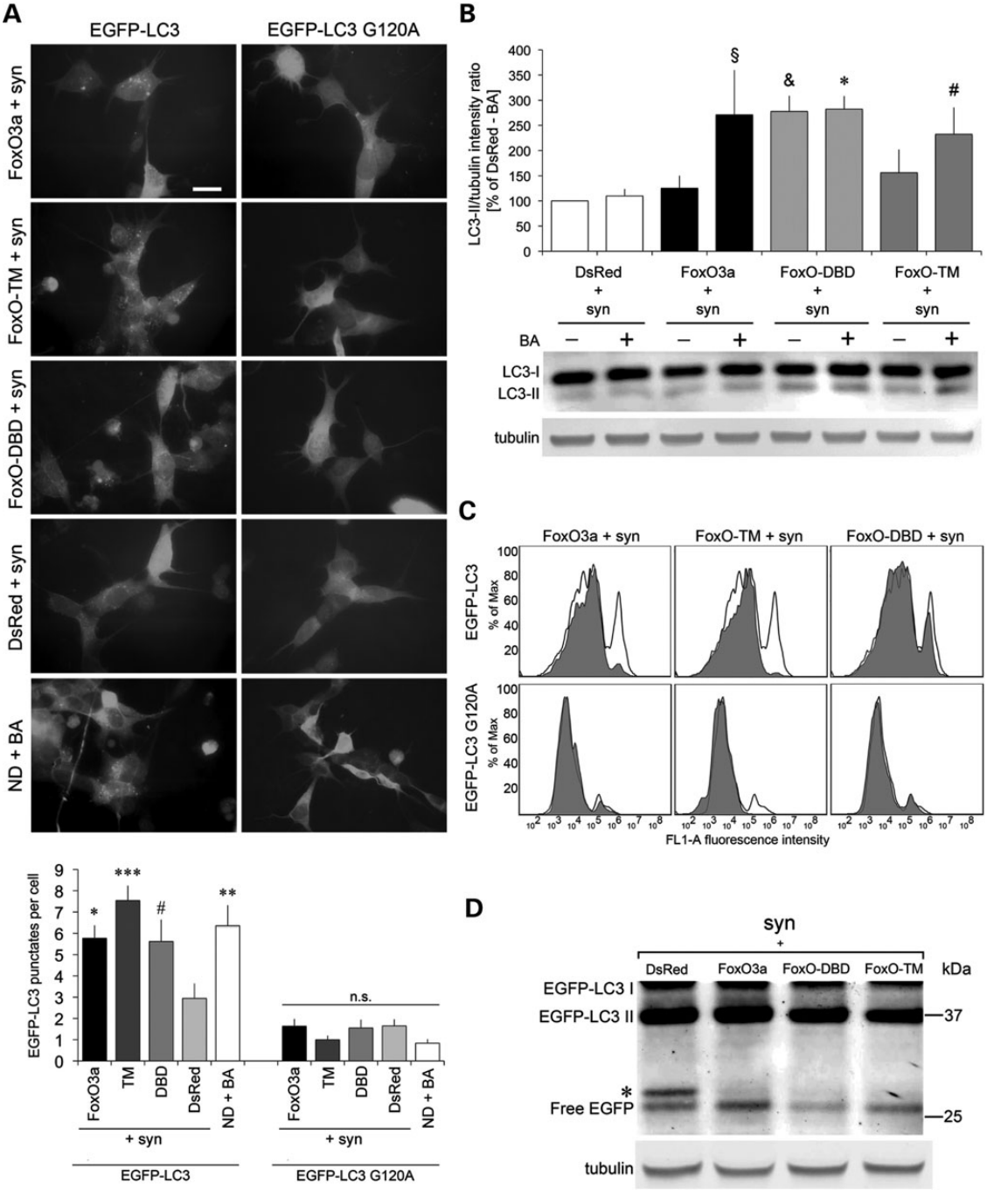

Figure 7. FOXO3 increases autophagic flux, and the dominant-negative FoxO-DBD inhibits lysosomal degradation in SH-SY5Y cells expressing α-synuclein. (**A**) Effect of vectors modulating FOXO3 activity in SH-SY5Y cells infected with either AAV2/6-PGK-EGFP-LC3 or G120A vectors. At 48 h post-infection, fluorescent puncta representing autophagosomes are increased with all FOXO vectors as compared with the DsRed2 control, and similarly to the nutrient deprivation group (ND) treated with BA. Scale bar: 20 μm. Statistical analysis: $n = 3$, one-way ANOVA with Fisher's LSD *post hoc* test, $^{\#}P = 0.026$, $^{*}P = 0.019$, $^{**}P = 0.005$, $^{***}P = 0.0001$ relative to DsRed. (**B**) Western blot analysis of protein extracts taken from SH-SY5Y cells infected with AAV2/6-CMV-FoxO variants or AAV2/6-CMV-DsRed, with and without BA. Membrane was probed with an anti-LC3B or anti-tubulin antibody as indicated. Graph represents the relative band intensity of LC3-II/tubulin. Note the difference in band intensity with and without BA in the active forms (FoxO3a and FoxO-TM), whereas there is no difference with FoxO-DBD 48 h post-infection. Statistical analysis: $n = 3$, one-way ANOVA with Fisher's LSD *post hoc* test, $^{\S}P = 0.019$, $^{*}P = 0.013$, $^{\#}P = 0.064$ relative to DsRed + BA and $\&P = 0.011$ relative to DsRed-BA. (**C**) Flow cytometry analysis of EGFP-LC3 and G120A expressing stable cell line infected with either the AAV2/6-CMV-FoxO forms (shaded traces) or AAV2/6-CMV-DsRed (open traces) 48 h post-infection. There is no decrease in fluorescence intensity of EGFP-LC3 in the FoxO-DBD group ($n = 3$). (**D**) Western blot analysis of protein extracts from infected SH-SY5Y cells stably expressing EGFP-LC3 48 h post-infection. Membrane was probed with an anti-GFP or anti-tubulin antibody. The band intensity of free EGFP is an indicator for autophagic flux, which is reduced in the FoxO-DBD group ($n = 4$).

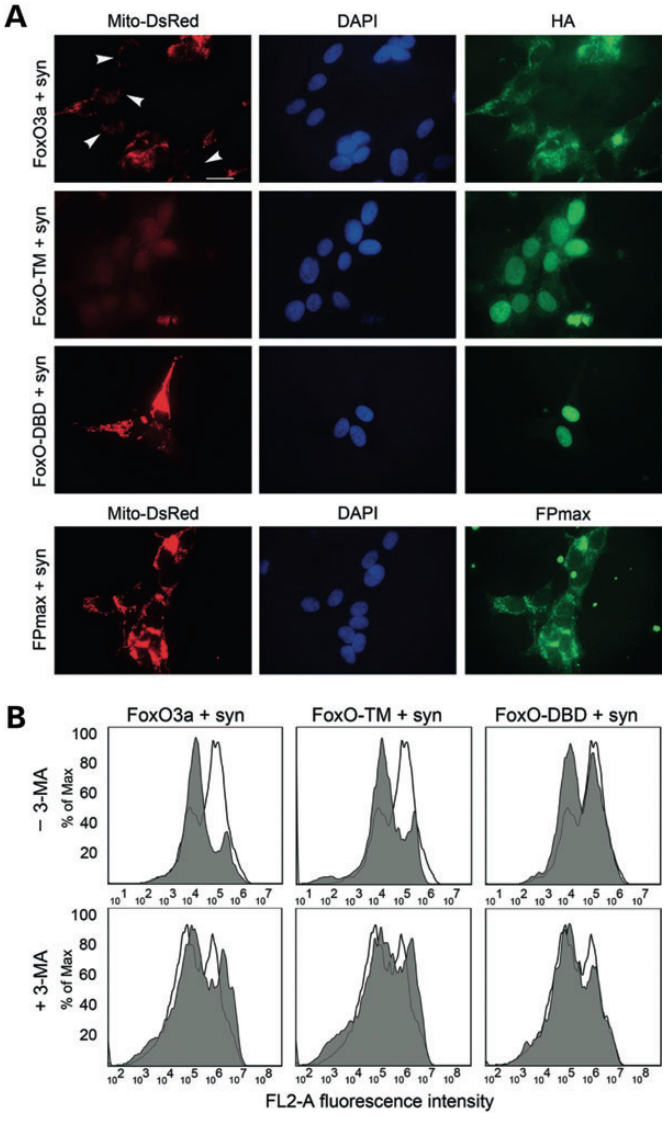

Figure 8. Active forms of FOXO3, but not FoxO-DBD, reduce the overall number of Mito-DsRed-labeled mitochondria in SH-SY5Y-expressing α-synuclein. (**A**) Immunostaining for HA, DAPI and Mito-DsRed 72 h post-infection shows a marked reduction of Mito-DsRed fluorescence in the FoxO-TM group and a decrease in some cells expressing FOXO3 (arrowheads). HA staining demonstrates the nuclear localization of FoxO-TM and FoxO-DBD at this time point. Scale bar: 20 μm. (**B**) Flow cytometry analysis of Mito-DsRed signal in SH-SY5Y infected with either FoxO3a vectors (shaded traces) or the FPmax control (open traces), with and without 3-MA, an autophagy inhibitor. There is a significant shift toward a low fluorescent population with FoxO3a and FoxO-TM that is not observed with FoxO-DBD or in any condition with 3-MA 72 h post-infection (representative result for $n = 3$).

Mito-DsRed. Although we did not detect any significant change in Mito-DsRed fluorescence at 48 h (Supplementary Material, Fig. S8B), we noticed a dramatic reduction in the fluorescence signal at 72 h in the FoxO3a and FoxO-TM conditions compared with the FPmax control, but not with FoxO-DBD (Fig. 8B).

To see if this effect was due to autophagic degradation of mitochondria, we incubated the cells with 3-methyladenine (3-MA) for 24 h. 3-MA is a PI3K inhibitor that blocks autophagy upstream of autophagosome formation (39). With 3-MA, none of the FOXO conditions (shaded traces) exhibited a large effect compared with the FPmax control (open traces) (Fig. 8A). This suggests that the reduction in Mito-DsRed fluorescence with FoxO3a and FoxO-TM is likely due to autophagic elimination of mitochondria.

DISCUSSION

These experiments address the role of FOXO3 transcriptional activity in the survival of nigral DA neurons, both in the normal brain and in conditions of α-synuclein accumulation that replicate neurodegenerative features of PD. Nigral DA neurons appear selectively vulnerable to variations in FOXO3 activity. Indeed, the constitutive activation of FOXO3 invariably leads to acute neuronal death. Nevertheless, FOXO3 also contributes to ROS detoxification in conditions of chronic oxidative stress, as demonstrated by oxidative damage that results from competitive FOXO inhibition. We find that the survival of DA neurons critically depends on tight FOXO regulation and explore the role of FOXO3 in neurons confronted to α-synuclein proteotoxicity. In the neuronal soma, increased FOXO3 activity leads to condensation of dense and large-sized aggregates, which stain positively for α-synuclein. Conversely, the level of α-synuclein appears significantly reduced in the most soluble protein fractions, which is consistent with the induction of autophagic degradation. In the condition of moderate FOXO3 activation induced by the wild-type form of the transcription factor, the reduction in soluble α-synuclein coincides with neuronal protection. Although FOXO3 reduces the overall load of α-synuclein, its transcriptional activity may also ultimately contribute to α-synuclein-induced neuronal loss, as demonstrated by the significant neuronal protection observed with the negative competitor FoxO-DBD.

We address the role of FOXO3 in the selectively vulnerable DA neurons of the SNpc. These neurons appear particularly sensitive to changes brought upon by the activity of FOXO3. Neuronal cell death observed in conditions of constitutive, Akt-independent activation of FOXO3 is consistent with the previously reported role of FOXO3 in inducing an apoptotic response in motor and sympathetic neurons via proapoptotic factors such as Fas ligand or Bim (21,40). However, we find that nigral neurons can tolerate overexpression of wild-type FOXO3, provided they are not exposed to stress stimuli which dictate the induction of neuronal death through complex regulatory modifications of FOXO (10). In nigral neurons, chronic exposure to oxidative stress generated by DA metabolism may likely contribute to lowering the threshold for FOXO3 to exert a potent proapoptotic activity.

Conversely, a high vector dose of the dominant-negative FoxO-DBD leads to a significant loss of neurons and striatal nerve terminals positive for TH. In this experimental condition, we observe the intraneuronal accumulation of HNE, a product of lipid peroxidation. HNE is implicated in neurodegenerative diseases such as PD, and was shown to modify α-synuclein, impacting on the aggregation of the protein (41,42). Therefore, the transcriptional activity of FOXO3 may have an important physiological role in nigral neurons by conferring resistance to oxidative stress, consistent with its role in the expression of genes implicated in ROS detoxification (22–24). This role of FOXO3 contrasts with the anti-apoptotic effect of FoxO-DBD

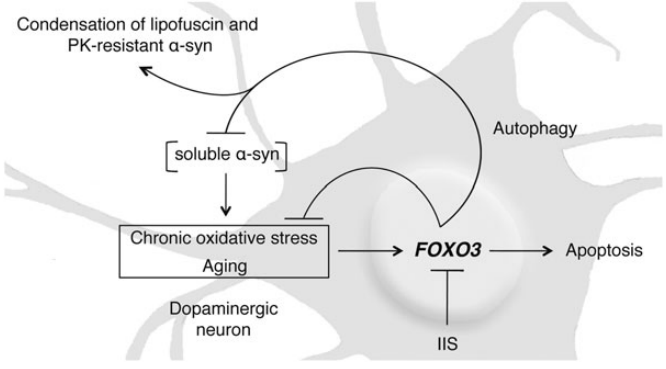

Figure 9. Proposed model for the role of FOXO3 in α-synuclein proteotoxicity. With age and degenerative disease, dopaminergic neurons are exposed to increased levels of α-synuclein and chronic oxidative stress. FOXO3 reduces α-synuclein proteotoxicity through the clearance of soluble α-synuclein and promotes the condensation of insoluble material that may contain inert forms of fibrillar α-synuclein. However, the overactivation of FOXO3 could ultimately be a mediator of neuronal cell death as demonstrated by the proapoptotic activity of the constitutively active form FoxO-TM and the neuronal protection observed with the dominant-negative FoxO-DBD.

in SH-SY5Y neuroblastoma cells subjected to acute oxidative stress. However, the nature of the stress caused by exposure to hydrogen peroxide at high concentration is likely to be very different from the chronic oxidative stress found in nigral dopaminergic neurons *in vivo*, and could favor the proapoptotic effects of FOXO. In α-synuclein-induced pathological conditions, FoxO-DBD also demonstrates protective effects. FOXO activity is increased in PD brain tissue (27), as well as in a *C. elegans* model of the α-synuclein pathology (43), and LRRK2 has been shown to activate FOXO (44). It is therefore possible that FOXO contributes to neuronal cell loss in PD pathology (Fig. 9). Overall, these results illustrate the dual role of FOXO, which promotes either apoptosis or resistance to stress, as a function of cell type and severity of the stress stimulus (16).

The overabundance of α-synuclein is consistently associated with the risk of developing PD. The finding that multiplications of the human α-synuclein gene lead to an acute form of autosomal dominant PD most convincingly supports this causal link. Oxidative stress combined with aging further contributes to the pathogenic activity of α-synuclein (45,46). FOXO3 reduces the level of soluble α-synuclein and promotes the condensation of insoluble material in the neuronal perikarya, staining positively for PK-resistant forms of α-synuclein and ThioS. In addition, IEM reveals large accumulations of insoluble material akin to lipofuscin. The decreased level of soluble α-synuclein could underlie the neuroprotection induced by wild-type FOXO3 (Fig. 9). The observed condensation of insoluble material appears consistent with the effect of DAF-16/FOXO in both *C. elegans* and mouse models of Alzheimer's disease Indeed, FOXO activity protects worms from Aβ-mediated proteotoxicity in conditions of reduced IIS, by increasing the formation of HMW forms of aggregated Aβ which are considered more inert (28). In APP/PS1 mice, reduced IIS protects from disease symptoms and induces the sequestration of soluble Aβ oligomers into dense, less toxic amyloid plaques (47). Our results further highlight a conserved role for FOXO in the condensation of potentially harmful insoluble end products of protein aggregation, organelle turnover and cellular metabolism. Such a mechanism may clear toxic oligomeric protein species from the cytosol and facilitate their elimination by autophagy.

Constitutive FOXO3 activation in rat DA neurons induces a clear accumulation of autophagic vacuoles coinciding with a reduction in mitochondrial content. *In vitro*, FOXO3 controls autophagic flux in SH-SY5Y cells. These results point to FOXO3 as an important mediator of autophagic degradation in adult DA neurons, consistent with the observed changes in α-synuclein abundance. FOXO3 similarly activates autophagy in muscle tissue in response to fasting or denervation by transactivating autophagy-related genes (26,48,49). Interestingly, acetylated FOXO1 is also able to upregulate autophagy independently of transcriptional activity, through cytosolic interaction with Atg7 (50). It is however unknown if FOXO3 can have any similar role. Recently, FOXO was also found to activate autophagy by transcriptionally regulating glutamine synthetase (51). In quiescent hematopoietic stem cells, FOXO3 has a critical role in the induction of autophagy to maintain energy levels during aging (52). It is therefore possible that similar mechanisms exist in energy-demanding neuronal populations that need to survive for the entire lifespan. Concomitant with the induction of autophagy, we have observed a reduction in mitochondrial content, particularly when FOXO3 is constitutively activated. It is unclear if mitochondrial loss is caused by non-specific macroautophagy or mitophagy, the selective elimination of dysfunctional mitochondria. The finding that Pink1 is a downstream target of FOXO3 supports a possible role in mitophagy (53), which will need to be further addressed.

Biochemical semi-quantitative assessment of protein levels in the SN reveals a reduction in the abundance of α-synuclein in response to FOXO3 overexpression. This effect is most evident on monomeric α-synuclein accumulating in highly soluble protein fractions. In addition, there is a clear reduction in PK-resistant α-synuclein immunoreactivity in striatal axon terminals. α-Synuclein can be cleared by autophagy and its pathogenic accumulation could be linked to impaired lysosomal autophagic activity (54–56). Therefore, it is possible that FOXO3 controls neuronal α-synuclein levels via autophagic degradation. Our results suggest that FOXO3 may primarily reduce the steady-state levels of the soluble forms of the protein. The fact that levels of insoluble α-synuclein remain unchanged despite lower amounts of soluble α-synuclein indicates that the transition toward insoluble α-synuclein aggregates may be accelerated.

Addressing the role of aging in neurodegenerative disorders is an immensely complex task, and the molecular processes at hand remain poorly understood. Accumulation of insoluble material, oxidative damage and neuronal apoptosis constitute the typical signature of normal and diseased brain aging. The role of FOXO at the intersection of these processes underlines its implication in neuronal degeneration. The finding that single genes can influence longevity raises the possibility to rationally control the impact of cellular senescence on age-related diseases (8). However, the role of these genes appears to be multifaceted, illustrating the complexity of the aging process. Further research is therefore warranted to elucidate how the interaction between aging and disease-causing factors dictates neuronal degeneration.

MATERIALS AND METHODS

Plasmid construction

Using standard cloning procedures, the cDNAs-encoding human FOXO3 (NM_001455.3), FoxO-TM and FoxO-DBD were subcloned into the pAAV-CMV-MCS backbone. An N-terminal HA tag was fused to FOXO-coding sequences and the three sites of Akt-dependent phosphorylation (Thr-32, Ser-253 and Ser-315) were replaced with alanine residues in the FoxO-TM form (30). The cDNA coding for the green fluorescent protein FPmax, which was amplified by PCR from the pmaxFP-PRL plasmid (Lonza, Basel, Switzerland), was subcloned into the pAAV-CMV-MCS backbone. The human wild-type α-synuclein gene (NM_000345.3), the EGFP-LC3B and EGFP-LC3B G120A cDNAs were subcloned into the pAAV-PGK-MCS backbone modified from the pAAV-CMV-MCS vector.

AAV2/6 virus production and titration

AAV2/6 recombinant viral particles were produced and titered as previously described (57,58). The titers measured for all AAV2/6 preparations were in the range of $3-20 \times 10^{10}$TU/ml.

Stereotaxic injections into the rat SNpc and GP

Animal experiments were approved by a local Ethics committee and carried out in accordance with Swiss laws on animal experimentation and the European Community Council directive (86/609/EEC) for the care and use of laboratory animals. Stereotaxic injections were performed following previously described methods (58).

Immunohistological analysis and quantification

Preparation of brain section, 3 or 12 weeks post-injection was performed as previously described (58). Immunohistochemistry was achieved by standard procedures. Image processing and analysis were determined as described in our publications (59, 60). Antibody information is provided in Supplementary Material Experimental Procedures.

Western blot analysis

Human α-synuclein extraction from dissected SNpc

Sixteen weeks post-injection, SNpc cryosections were prepared as previously described (59). They were sequentially extracted with buffers designed to increasingly solubilize α-synuclein. At each step, homogenization in an appropriate buffer which contained protease inhibitors (Roche Pharma) was followed by centrifugation at 175 000*g* for 30 min at 4°C. The supernatant was then removed and the pellet was homogenized in the next extraction buffer. Sequential extraction was made in Hepes buffer (50 mM Hepes, pH 7.4), 1% NP40 (50 mM Hepes, pH 7.4; 150 mM NaCl; NP40 1%), and 2% SDS (50 mM Hepes, pH 7.4; 150 mM NaCl; SDS 2%). Finally, the SDS-insoluble pellets were extracted overnight with guanidine buffer (50 mM Hepes, pH 7.4; 5 mM EDTA; 8 M guanidine–HCl; 5 mM DTT) before 5 min incubation at 50°C and centrifugation at 20 000*g* for 1 h at RT. The resulting supernatant was precipitated in 100% ethanol at −80°C for 10 min, centrifuged at 15 000*g* for 5 min at 4°C and resuspended in sample buffer (37.5 mM Tris–HCl, pH 7.0, 3% SDS; 1.5% mercaptoethanol; 7.5% glycerol; 0.013% Coomassie blue G-250). Protein concentrations were determined using the BCA Protein Assay Kit (Pierce, Rockford, IL, USA).

Immunoblotting

Equal amounts of proteins were loaded on SDS–PAGE, transferred to nitrocellulose and probed with specified primary antibodies, as described in the Supplementary Material Experimental Procedures. Blue Native-PAGE was performed on Bis–Tris Gel. Proteins were transferred to PVDF membranes and probed with the Syn211 antibody. 2D native-PAGE/SDS–PAGE was performed running a first dimensional native-PAGE, followed by a second dimensional SDS–PAGE. Proteins were transferred to a nitrocellulose and probed with the syn1 antibody. Infrared Imaging (Odyssey, Li-Cor) was used for the detection and the ImageJ software for the semi-quantitative analysis of signal density (http://rsb.info.nih.gov/ij/).

Detection of LC3-I and -II, and p62/SQSTM1 in SH-SY5Y cells

SH-SY5Y cells differentiated in N2 medium were infected with the AAV-PGK-kz-α-synuclein-WPRE vector (1×10^7 TU), or with AAV-CMV-FoxO3a, FoxO-TM, FoxO-DBD or DsRed2 (3×10^6 TU). If needed, the total amount of vector was balanced by adding non-coding AAV-PGK-MCS-WPRE vector in the corresponding wells. To inhibit lysosomal degradation, Bafilomycin A1 was added 24 h later, to a final concentration of 10 nM per well. The cells were collected 48 h post-infection in 1% SDS before sonication at 50% intensity at 1 s intervals for 10 s and boiled at 95°C for 10 min. Samples were loaded on NuPAGE gel, transferred to PVDF membrane and probed with an anti-MAP1LC3B (Lifespan BioSciences). The extraction procedure and blotting were similar for the analysis of EGFP-LC3 lysosomal degradation, using an anti-EGFP antibody (rabbit IgG 1/2000; ab290, Abcam, Cambridge, UK). For immunodetection of p62/SQSTM1, the membrane was probed with anti-p62 (guinea pig 1/1000; Progen, Heidelberg, Germany).

Immuno-electron microscopy

Sixteen weeks post-injection, one rat per group was deeply anesthetized with sodium pentobarbital and perfused transcardially with 0.1% glutaraldehyde, 4% PFA. Brains were rapidly removed and 50 μm vibratome (Leica VT1200) sections cut coronally through the SNpc. Slices were then treated using a pre-embedding protocol as described previously (61). Anti-α-synuclein LB509 was used as a primary antibody, which was revealed by a gold-labeled secondary antibody. Ultrastructural studies were performed on ultrathin sections (60 nm), stained with lead citrate and uranyl acetate and viewed with a Philips CM10 transmission electron microscope. ImageJ software was used to quantify the number of mitochondria and autophagic vacuoles per arbitrary unit of cytosol.

Oxidative stress assay and quantification

SH-SY5Y cells differentiated in N2 medium in laminin-coated 6-wells were infected with AAV-CMV-FoxO3a, FoxO-TM or

FoxO-DBD. Forty-eight hours later, the cells were treated with 200 μM of H_2O_2 for 6 h. For a positive control condition, some cells were treated for 23 h with 100 nM epoxomycin. The cells were resuspended in 10 mM Hepes/NaOH, pH 7.4, 140 mM NaCl, 2.5 mM $CaCl_2$, and 3 mg/ml Annexin V. After 15 min of incubation, cell death was quantified by flow cytometry (CyAn ADP, Beckman Coulter) and analyzed on FlowJo software (Tree Star, Ashland, OR, USA).

Cellular assays for autophagy

For inhibition of autophagy, cells were treated either with 10 mM 3-MA (Sigma, St. Louis, MO, USA) or 65 nM bafilomycin A1 for 4 h (Sigma).

N2-differentiated SH-SY5Y cells in laminin/poly-L-lysine-coated wells were infected with either EGFP-LC3 or G120A vector. The cells were also infected with AAV-CMV-FoxO3a, FoxO-TM, FoxO-DBD or DsRed2 virus and AAV-PGK-kz-α-synuclein-WPRE vectors. At 48 h post-infection, the cells were fixed with 4% PFA for 15 min and mounted using VectaShield with DAPI (Vector, Burlingame, CA, USA). For the nutrient deprivation condition, the cells were incubated for 4 h in DMEM only.

Establishment of stable cell lines

EGFP-LC3, EGFP-LC3 G120A and Mito-DsRed2 plasmids were transfected into SH-SY5Y cells using the Microporator MP-100 (Invitrogen) according to manufacturer's instruction. Stable cell lines were established by growing cells in medium with 800 μg/ml of Geneticin (Invitrogen). The cells were subsequently subcloned to ensure uniform fluorescence. The fluorescence signal of EGFP or Mito-DsRed2 was quantified by flow cytometry. Immunocytochemistry is described in Supplementary Material, Experimental Procedures.

Statistical analyses

Depending upon the experimental paradigm, we performed either one- or two-way factorial ANOVA. The ANOVA was followed by a Newman–Keuls *post hoc* test, unless specified. For analysis of signal density in western blots and number of autophagic puncta, a Fisher's LSD *post hoc* test was applied. Kruskal–Wallis one-way ANOVA was performed for analysis of organelle density by electron microscopy. Statistical analyses were made using the Statistica software (StatSoft, France). Significance level was set at $P < 0.05$. Data are expressed as average ± SEM.

A complete description of experimental procedures and supplementary figures is provided asSupplementary Material.

SUPPLEMENTARY MATERIAL

Supplementary Material is available at *HMG* online.

ACKNOWLEDGEMENTS

The authors thank Philippe Colin, Viviane Padrun, Fabienne Pidoux, Christel Sadeghi and Aline Aebi for their valuable technical assistance. We are also grateful to Thierry Laroche and José Artacho from the BioImaging and Optics platform for their expert technical support. We thank Dr Boudewijn Burgering for providing the FOXO luciferase reporter construct.

Conflict of Interest statement: None declared.

FUNDING

This work was supported by the Swiss National Science Foundation [grant numbers 31003A_120653, 135696].

REFERENCES

1. Conway, K.A., Lee, S.J., Rochet, J.C., Ding, T.T., Williamson, R.E. and Lansbury, P.T. Jr. (2000) Acceleration of oligomerization, not fibrillization, is a shared property of both alpha-synuclein mutations linked to early-onset Parkinson's disease: implications for pathogenesis and therapy. *Proc. Natl. Acad. Sci. USA*, **97**, 571–576.
2. Lashuel, H.A., Petre, B.M., Wall, J., Simon, M., Nowak, R.J., Walz, T. and Lansbury, P.T. Jr (2002) Alpha-synuclein, especially the Parkinson's disease-associated mutants, forms pore-like annular and tubular protofibrils. *J. Mol. Biol.*, **322**, 1089–1102.
3. Polymeropoulos, M.H., Lavedan, C., Leroy, E., Ide, S.E., Dehejia, A., Dutra, A., Pike, B., Root, H., Rubenstein, J., Boyer, R. *et al.* (1997) Mutation in the alpha-synuclein gene identified in families with Parkinson's disease. *Science*, **276**, 2045–2047.
4. Singleton, A.B., Farrer, M., Johnson, J., Singleton, A., Hague, S., Kachergus, J., Hulihan, M., Peuralinna, T., Dutra, A., Nussbaum, R. *et al.* (2003) Alpha-synuclein locus triplication causes Parkinson's disease. *Science*, **302**, 841.
5. Chartier-Harlin, M.C., Kachergus, J., Roumier, C., Mouroux, V., Douay, X., Lincoln, S., Levecque, C., Larvor, L., Andrieux, J., Hulihan, M. *et al.* (2004) Alpha-synuclein locus duplication as a cause of familial Parkinson's disease. *Lancet*, **364**, 1167–1169.
6. Harman, D. (1956) Aging: a theory based on free radical and radiation chemistry. *J. Gerontol.*, **11**, 298–300.
7. Storz, P. (2006) Reactive oxygen species-mediated mitochondria-to-nucleus signaling: a key to aging and radical-caused diseases. *Sci. STKE*, **2006**, re3.
8. Kenyon, C. (2005) The plasticity of aging: insights from long-lived mutants. *Cell*, **120**, 449–460.
9. Masoro, E.J. (2000) Caloric restriction and aging: an update. *Exp. Gerontol.*, **35**, 299–305.
10. Greer, E.L. and Brunet, A. (2005) FOXO Transcription factors at the interface between longevity and tumor suppression. *Oncogene*, **24**, 7410–7425.
11. Chung, W.H., Dao, R.L., Chen, L.K. and Hung, S.I. (2010) The role of genetic variants in human longevity. *Ageing Res. Rev.*, **9**(Suppl. 1), S67–S78.
12. Kenyon, C., Chang, J., Gensch, E., Rudner, A. and Tabtiang, R. (1993) A *C. elegans* mutant that lives twice as long as wild type. *Nature*, **366**, 461–464.
13. Kimura, K.D., Tissenbaum, H.A., Liu, Y. and Ruvkun, G. (1997) daf-2, an insulin receptor-like gene that regulates longevity and diapause in *Caenorhabditis elegans*. *Science*, **277**, 942–946.
14. Brunet, A., Sweeney, L.B., Sturgill, J.F., Chua, K.F., Greer, P.L., Lin, Y., Tran, H., Ross, S.E., Mostoslavsky, R., Cohen, H.Y. *et al.* (2004) Stress-dependent regulation of FOXO transcription factors by the SIRT1 deacetylase. *Science*, **303**, 2011–2015.
15. Wang, F., Nguyen, M., Qin, F.X. and Tong, Q. (2007) SIRT2 deacetylates FOXO3a in response to oxidative stress and caloric restriction. *Aging Cell*, **6**, 505–514.
16. Lehtinen, M.K., Yuan, Z., Boag, P.R., Yang, Y., Villen, J., Becker, E.B., DiBacco, S., de la Iglesia, N., Gygi, S., Blackwell, T.K. *et al.* (2006) A conserved MST-FOXO signaling pathway mediates oxidative-stress responses and extends life span. *Cell*, **125**, 987–1001.
17. Oh, S.W., Mukhopadhyay, A., Svrzikapa, N., Jiang, F., Davis, R.J. and Tissenbaum, H.A. (2005) JNK Regulates lifespan in *Caenorhabditis elegans* by modulating nuclear translocation of forkhead transcription factor/DAF-16. *Proc. Natl. Acad. Sci. USA*, **102**, 4494–4499.
18. Greer, E.L., Oskoui, P.R., Banko, M.R., Maniar, J.M., Gygi, M.P., Gygi, S.P. and Brunet, A. (2007) The energy sensor AMP-activated protein kinase

directly regulates the mammalian FOXO3 transcription factor. *J. Biol. Chem.*, **282**, 30107–30119.
19. Tran, H., Brunet, A., Grenier, J.M., Datta, S.R., Fornace, A.J. Jr, DiStefano, P.S., Chiang, L.W. and Greenberg, M.E. (2002) DNA repair pathway stimulated by the forkhead transcription factor FOXO3a through the Gadd45 protein. *Science*, **296**, 530–534.
20. Sandri, M., Sandri, C., Gilbert, A., Skurk, C., Calabria, E., Picard, A., Walsh, K., Schiaffino, S., Lecker, S.H. and Goldberg, A.L. (2004) Foxo transcription factors induce the atrophy-related ubiquitin ligase atrogin-1 and cause skeletal muscle atrophy. *Cell*, **117**, 399–412.
21. Gilley, J., Coffer, P.J. and Ham, J. (2003) FOXO transcription factors directly activate bim gene expression and promote apoptosis in sympathetic neurons. *J. Cell Biol.*, **162**, 613–622.
22. Kops, G.J., Dansen, T.B., Polderman, P.E., Saarloos, I., Wirtz, K.W., Coffer, P.J., Huang, T.T., Bos, J.L., Medema, R.H. and Burgering, B.M. (2002) Forkhead transcription factor FOXO3a protects quiescent cells from oxidative stress. *Nature*, **419**, 316–321.
23. Paik, J.H., Ding, Z., Narurkar, R., Ramkissoon, S., Muller, F., Kamoun, W.S., Chae, S.S., Zheng, H., Ying, H., Mahoney, J. *et al.* (2009) Foxos cooperatively regulate diverse pathways governing neural stem cell homeostasis. *Cell Stem Cell*, **5**, 540–553.
24. Renault, V.M., Rafalski, V.A., Morgan, A.A., Salih, D.A., Brett, J.O., Webb, A.E., Villeda, S.A., Thekkat, P.U., Guillerey, C., Denko, N.C. *et al.* (2009) Foxo3 regulates neural stem cell homeostasis. *Cell Stem Cell*, **5**, 527–539.
25. Brunet, A., Bonni, A., Zigmond, M.J., Lin, M.Z., Juo, P., Hu, L.S., Anderson, M.J., Arden, K.C., Blenis, J. and Greenberg, M.E. (1999) Akt promotes cell survival by phosphorylating and inhibiting a forkhead transcription factor. *Cell*, **96**, 857–868.
26. Zhao, J., Brault, J.J., Schild, A., Cao, P., Sandri, M., Schiaffino, S., Lecker, S.H. and Goldberg, A.L. (2007) Foxo3 coordinately activates protein degradation by the autophagic/lysosomal and proteasomal pathways in atrophying muscle cells. *Cell Metab.*, **6**, 472–483.
27. Dumitriu, A., Latourelle, J.C., Hadzi, T.C., Pankratz, N., Garza, D., Miller, J.P., Vance, J.M., Foroud, T., Beach, T.G. and Myers, R.H. (2012) Gene expression profiles in Parkinson disease prefrontal cortex implicate FOXO1 and genes under its transcriptional regulation. *PLoS Genet.*, **8**, e1002794.
28. Cohen, E., Bieschke, J., Perciavalle, R.M., Kelly, J.W. and Dillin, A. (2006) Opposing activities protect against age-onset proteotoxicity. *Science*, **313**, 1604–1610.
29. Morley, J.F., Brignull, H.R., Weyers, J.J. and Morimoto, R.I. (2002) The threshold for polyglutamine-expansion protein aggregation and cellular toxicity is dynamic and influenced by aging in Caenorhabditis elegans. *Proc. Natl. Acad. Sci. USA*, **99**, 10417–10422.
30. Brunet, A., Park, J., Tran, H., Hu, L.S., Hemmings, B.A. and Greenberg, M.E. (2001) Protein kinase SGK mediates survival signals by phosphorylating the forkhead transcription factor FKHRL1 (FOXO3a). *Mol. Cell. Biol.*, **21**, 952–965.
31. Tothova, Z., Kollipara, R., Huntly, B.J., Lee, B.H., Castrillon, D.H., Cullen, D.E., McDowell, E.P., Lazo-Kallanian, S., Williams, I.R., Sears, C. *et al.* (2007) Foxos are critical mediators of hematopoietic stem cell resistance to physiologic oxidative stress. *Cell*, **128**, 325–339.
32. Xie, Q., Hao, Y., Tao, L., Peng, S., Rao, C., Chen, H., You, H., Dong, M.Q. and Yuan, Z. (2012) Lysine methylation of FOXO3 regulates oxidative stress-induced neuronal cell death. *EMBO Rep.*, **13**, 371–377.
33. Sulzer, D., Mosharov, E., Talloczy, Z., Zucca, F.A., Simon, J.D. and Zecca, L. (2008) Neuronal pigmented autophagic vacuoles: lipofuscin, neuromelanin, and ceroid as macroautophagic responses during aging and disease. *J. Neurochem.*, **106**, 24–36.
34. Choubey, V., Safiulina, D., Vaarmann, A., Cagalinec, M., Wareski, P., Kuum, M., Zharkovsky, A. and Kaasik, A. (2011) Mutant A53T alpha-synuclein induces neuronal death by increasing mitochondrial autophagy. *J. Biol. Chem.*, **286**, 10814–10824.
35. Mizushima, N., Yoshimori, T. and Levine, B. (2010) Methods in mammalian autophagy research. *Cell*, **140**, 313–326.
36. Tanida, I., Yamaji, T., Ueno, T., Ishiura, S., Kominami, E. and Hanada, K. (2008) Consideration about negative controls for LC3 and expression vectors for four colored fluorescent protein-LC3 negative controls. *Autophagy*, **4**, 131–134.
37. Shvets, E., Fass, E. and Elazar, Z. (2008) Utilizing flow cytometry to monitor autophagy in living mammalian cells. *Autophagy*, **4**, 621–628.
38. Gao, W., Ding, W.X., Stolz, D.B. and Yin, X.M. (2008) Induction of macroautophagy by exogenously introduced calcium. *Autophagy*, **4**, 754–761.
39. Seglen, P.O. and Gordon, P.B. (1982) 3-Methyladenine: specific inhibitor of autophagic/lysosomal protein degradation in isolated rat hepatocytes. *Proc. Natl. Acad. Sci. USA*, **79**, 1889–1892.
40. Barthelemy, C., Henderson, C.E. and Pettmann, B. (2004) Foxo3a induces motoneuron death through the Fas pathway in cooperation with JNK. *BMC Neurosci.*, **5**, 48.
41. Qin, Z., Hu, D., Han, S., Reaney, S.H., Di Monte, D.A. and Fink, A.L. (2007) Effect of 4-hydroxy-2-nonenal modification on alpha-synuclein aggregation. *J. Biol. Chem.*, **282**, 5862–5870.
42. Xiang, W., Schlachetzki, J.C., Helling, S., Bussmann, J.C., Berlinghof, M., Schaffer, T.E., Marcus, K., Winkler, J., Klucken, J. and Becker, C.M. (2013) Oxidative stress-induced posttranslational modifications of alpha-synuclein: specific modification of alpha-synuclein by 4-hydroxy-2-nonenal increases dopaminergic toxicity. *Mol. Cell Neurosci.*, **54**, 71–83.
43. Kuwahara, T., Tonegawa, R., Ito, G., Mitani, S. and Iwatsubo, T. (2012) Phosphorylation of alpha-synuclein protein at Ser-129 reduces neuronal dysfunction by lowering its membrane binding property in *Caenorhabditis elegans*. *J. Biol. Chem.*, **287**, 7098–7109.
44. Kanao, T., Venderova, K., Park, D.S., Unterman, T., Lu, B. and Imai, Y. (2010) Activation of FoxO by LRRK2 induces expression of proapoptotic proteins and alters survival of postmitotic dopaminergic neuron in Drosophila. *Hum. Mol. Genet.*, **19**, 3747–3758.
45. Cookson, M.R. (2009) alpha-Synuclein and neuronal cell death. *Mol. Neurodegener.*, **4**, 9.
46. Xie, W., Wan, O.W. and Chung, K.K. (2010) New insights into the role of mitochondrial dysfunction and protein aggregation in Parkinson's disease. *Biochim. Biophys. Acta*, **1802**, 935–941.
47. Cohen, E., Paulsson, J.F., Blinder, P., Burstyn-Cohen, T., Du, D., Estepa, G., Adame, A., Pham, H.M., Holzenberger, M., Kelly, J.W. *et al.* (2009) Reduced IGF-1 signaling delays age-associated proteotoxicity in mice. *Cell*, **139**, 1157–1169.
48. Sengupta, A., Molkentin, J.D. and Yutzey, K.E. (2009) Foxo transcription factors promote autophagy in cardiomyocytes. *J. Biol. Chem.*, **284**, 28319–28331.
49. Mammucari, C., Milan, G., Romanello, V., Masiero, E., Rudolf, R., Del Piccolo, P., Burden, S.J., Di Lisi, R., Sandri, C., Zhao, J. *et al.* (2007) Foxo3 controls autophagy in skeletal muscle in vivo. *Cell Metab.*, **6**, 458–471.
50. Zhao, Y., Yang, J., Liao, W., Liu, X., Zhang, H., Wang, S., Wang, D., Feng, J., Yu, L. and Zhu, W.G. (2010) Cytosolic FoxO1 is essential for the induction of autophagy and tumour suppressor activity. *Nat. Cell Biol.*, **12**, 665–675.
51. van der Vos, K.E., Eliasson, P., Proikas-Cezanne, T., Vervoort, S.J., van Boxtel, R., Putker, M., van Zutphen, I.J., Mauthe, M., Zellmer, S., Pals, C. *et al.* (2012) Modulation of glutamine metabolism by the PI(3)K-PKB-FOXO network regulates autophagy. *Nat. Cell Biol.*, **14**, 829–837.
52. Warr, M.R., Binnewies, M., Flach, J., Reynaud, D., Garg, T., Malhotra, R., Debnath, J. and Passegue, E. (2013) FOXO3A Directs a protective autophagy program in haematopoietic stem cells. *Nature*, **494**, 323–327.
53. Mei, Y., Zhang, Y., Yamamoto, K., Xie, W., Mak, T.W. and You, H. (2009) FOXO3a-dependent Regulation of Pink1 (Park6) mediates survival signaling in response to cytokine deprivation. *Proc. Natl. Acad. Sci. USA*, **106**, 5153–5158.
54. Lee, H.J., Khoshaghideh, F., Patel, S. and Lee, S.J. (2004) Clearance of alpha-synuclein oligomeric intermediates via the lysosomal degradation pathway. *J. Neurosci.*, **24**, 1888–1896.
55. Webb, J.L., Ravikumar, B., Atkins, J., Skepper, J.N. and Rubinsztein, D.C. (2003) Alpha-synuclein is degraded by both autophagy and the proteasome. *J. Biol. Chem.*, **278**, 25009–25013.
56. Cuervo, A.M., Stefanis, L., Fredenburg, R., Lansbury, P.T. and Sulzer, D. (2004) Impaired degradation of mutant alpha-synuclein by chaperone-mediated autophagy. *Science*, **305**, 1292–1295.
57. Grimm, D., Kay, M.A. and Kleinschmidt, J.A. (2003) Helper virus-free, optically controllable, and two-plasmid-based production of adeno-associated virus vectors of serotypes 1 to 6. *Mol. Ther.*, **7**, 839–850.
58. Dusonchet, J., Bensadoun, J.C., Schneider, B.L. and Aebischer, P. (2009) Targeted overexpression of the parkin substrate Pael-R in the nigrostriatal system of adult rats to model Parkinson's disease. *Neurobiol. Dis.*, **35**, 32–41.
59. Azeredo da Silveira, S., Schneider, B.L., Cifuentes-Diaz, C., Sage, D., Abbas-Terki, T., Iwatsubo, T., Unser, M. and Aebischer, P. (2009) Phosphorylation does not prompt, nor prevent, the formation of

alpha-synuclein toxic species in a rat model of parkinson's disease. *Hum. Mol. Genet.*, **18**, 872–887.
60. Gaugler, M.N., Genc, O., Bobela, W., Mohanna, S., Ardah, M.T., El-Agnaf, O.M., Cantoni, M., Bensadoun, J.C., Schneggenburger, R., Knott, G.W. *et al.* (2012) Nigrostriatal overabundance of alpha-synuclein leads to decreased vesicle density and deficits in dopamine release that correlate with reduced motor activity. *Acta Neuropathol.*, **123**, 653–669.
61. Voutsinos-Porche, B., Knott, G., Tanaka, K., Quairiaux, C., Welker, E. and Bonvento, G. (2003) Glial glutamate transporters and maturation of the mouse somatosensory cortex. *Cereb. Cortex*, **13**, 1110–1121.